Possibilities for Breakeven and Ignition of D-^{3}He Fusion Fuel in a Near Term Tokamak

G.A. Emmert, L. El-Guebaly, G.L. Kulcinski, J.F. Santarius, J.E. Scharer, I.N. Sviatoslavsky, P.L. Walstrom, L.J. Wittenberg, R. Klingelhöfer

May 1989

UWFDM-799

Published in Nuclear Fusion, Vol. 29, No. 9 (1989), pp. 1427–1448.

FUSION TECHNOLOGY INSTITUTE

UNIVERSITY OF WISCONSIN

MADISON WISCONSIN

Possibilities for Breakeven and Ignition of D-^{3}He Fusion Fuel in a Near Term Tokamak

G.A. Emmert, L. El-Guebaly, G.L. Kulcinski, J.F. Santarius, J.E. Scharer, I.N. Sviatoslavsky, P.L. Walstrom, L.J. Wittenberg, R. Klingelhöfer

Fusion Technology Institute
University of Wisconsin
1500 Engineering Drive
Madison, WI 53706

http://fti.neep.wisc.edu

May 1989

UWFDM-799

Published in Nuclear Fusion, Vol. 29, No. 9 (1989), pp. 1427–1448.

POSSIBILITIES FOR BREAKEVEN AND IGNITION OF D-^{3}He FUSION FUEL IN A NEAR TERM TOKAMAK

G.A. Emmert, L.A. El-Guebaly, G.L. Kulcinski,
J.F. Santarius, J.E. Scharer, I.N. Sviatoslavsky,
P.L. Walstrom, L.J. Wittenberg

University of Wisconsin
Fusion Technology Institute
1500 Johnson Drive
Madison, WI 53706

and

R. Klingelhofer

Kernforschungszentrum Karlsruhe
Karlsruhe, Federal Republic of Germany

May 1989

UWFDM-799

Published in Nuclear Fusion, Vol. 29, No. 9 (1989), pp. 1427-1448.

1. INTRODUCTION

There has been renewed worldwide interest in the advanced fusion fuels which produce relatively low levels of radioactivity [1-4]. The major emphasis of this recent research has been on the D-^{3}He cycle for which neither the fuel nor reaction products are radioactive. Of course, side reactions of the deuterium fuel produce some neutrons, but the neutron production and the total induced radiation damage and radioactivity are reduced by 1 to 2 orders of magnitude from the DT case, depending on the fuel mixture.

The purpose of this paper is to consider operation with D-^{3}He in a near term tokamak of the NET/INTOR class. This report will concentrate on the physics results as opposed to the technological advantages of this fuel cycle, some of which are covered in other papers [1,2,5]. The approach taken here is to use the latest documented (1985) design of NET [6] as a base case to illustrate the physics results that can be obtained in a hot D-^{3}He plasma. We then consider variations of the NET design which can enhance the performance with D-^{3}He fuel.

The basic parameters of the NET tokamak (double null divertor configuration) are given in Reference 6. The NET team has also considered an enhanced plasma version with a major radius of 5.41 m. This latter version we label NET-EP. A few basic parameters of each are given in Table I.

2. PLASMA PERFORMANCE MODELLING

Before considering the detailed plasma physics calculations, it is worthwhile to compare D-^{3}He fusion with D-T fusion from the point of view of basic physics principles. This comparison is helpful in understanding the more detailed physics calculations.

The basic fusion reactions of interest are:

$$D + {}^3He \rightarrow {}^4He(3.6) + p(14.7) + 18.3\ MeV$$

$$D + T \rightarrow {}^4He(3.5) + n(14.1) + 17.6\ MeV\ .$$

The energy (in MeV) of each of the charged particle products are shown in parentheses. It is important that 100% of the energy released in the D-^{3}He reaction is in the form of charged particles which deposit their energy in the plasma and help maintain the plasma energy balance. For the D-T reaction,

only 20% of the energy released is in the alpha particle and is available for plasma heating. Because of the smaller mass of the proton, its gyroradius and banana widths are only twice that of a 3.6 MeV alpha particle. Hence finite orbit effects are not greatly increased over that of the D-T case. Fast ion losses due to trapping in the magnetic ripple is a concern for both D-^{3}He and D-T, but is larger in D-^{3}He because of the higher energy protons. This loss leads to bombardment of the first wall by fast ions and results in an increased local surface heat load. The severity of this heat load is a concern, but has not yet been established. Since all of the D-^{3}He fusion yield is in the form of charged particles and is deposited in the plasma, it is transferred to the first wall and divertor as surface heating. In a D-T plasma 80% of the fusion yield is in neutron energy which is deposited in the blanket and shield as volumetric heating. Consequently, the surface heat loads are higher in a D-^{3}He plasma for the same fusion power density in the plasma.

The Maxwellian-average $\langle\sigma v\rangle_f$ for the various fusion reactions are shown in Fig. 1. The $\langle\sigma v\rangle_f$ for D-^{3}He is much lower than that for D-T and peaks at a much higher plasma temperature. Of more interest in a β limited system is the figure of merit, $\langle\sigma v\rangle_f/T^2$, which is a measure of the power produced for a given β (ratio of the volume-averaged plasma pressure to the magnetic pressure) and magnetic field strength. This is shown in Fig. 2. We see that $\langle\sigma v\rangle_f/T^2$ for D-^{3}He peaks at 55 keV compared with 13 keV for the D-T reaction. In addition, the peak value for the D-^{3}He reaction is about a factor of 50 smaller than that for the D-T reaction. Also shown for comparison is the $\langle\sigma v\rangle_f/T^2$ for the D-D reaction; this is about a factor of 2 lower than the D-^{3}He value. Other factors (e.g. confinement scaling, volume averaging, and radiation losses) can shift the optimum temperature from the 55 keV peak, but the optimum will still be in the 50-80 keV range and not at the very high values implied by the maximum of $\langle\sigma v\rangle_f$.

In addition to the fusion reactivity, a concern is the degree of plasma confinement required for ignition; the usual figure of merit for this is the product of the density and the energy confinement time required for the plasma to be self-sustaining against power losses (loosely referred to as the "Lawson criteria"). Shown in Fig. 3 is $n\tau$ required for ignition versus the ion temperature; this energy confinement time measures the loss of energy by diffusion across the confining magnetic field. Bremsstrahlung and synchrotron radiation losses are included separately. Synchrotron radiation loss depends

not only on the magnetic field strength, density, and temperature, but also on the degree of re-absorption; the latter also introduces an additional magnetic field, density, temperature, size, and wall reflectivity dependence. Consequently, one cannot give a generic curve for $n\tau$ versus ion temperature. The density has been eliminated using the definition of beta (ratio of plasma pressure to magnetic field pressure), but the plasma minor radius has been chosen to be 2.5 m, the magnetic field at the plasma is 8 T, and the effective reflectivity is 0.8. These values are taken to be representative of a possible reactor. Also included in this $n\tau$ is the effect of the density and temperature profile in the plasma; both the density and temperature in Fig. 3 are volume-averaged. At low temperature bremsstrahlung dominates the losses; at higher temperature synchrotron radiation is more important. This is the reason for the beta dependence of the required $n\tau$ being larger at higher T_i. For beta = .1, the required $n\tau$ at the optimum ion temperature of 40 keV is about 1×10^{15} s/cm^3, which is about five times the required $n\tau$ for D-T fusion.

Because the ^{3}He part of the fuel has Z = 2, the electron density is a larger fraction of the total charged particle density than in a D-T plasma. This effect, coupled with the higher operating temperature for D-^{3}He, means that bremsstrahlung and synchrotron radiation play a larger role in the overall power balance than they do in the D-T plasma. In addition, the higher electron density reduces the allowed ion density for a given β and thereby reduces the fusion power density.

In a D-T plasma the optimum fuel mixture is 50% D and 50% T. In a D-^{3}He plasma, using a deuterium rich fuel mixture reduces the relative electron density and the radiation losses and improves the fusion power density. This is because, for every helium ion replaced by a deuterium ion, one electron is removed from the plasma. It turns out that the optimum fuel mixture is about 65% D and 35% ^{3}He.

Increasing the deuterium concentration in the fuel increases the neutron production rate. Neutrons are produced directly by the D(d,n)^{3}He reaction and indirectly by the reaction chain D(d,p)T, T(d,n)^{4}He. Although this chain is a two-step process it is significant because of the large D-T cross-section. It is also significant because this neutron has an energy of 14 MeV while the neutron produced in the D-D reaction has an energy of 2.45 MeV. The branching ratio between the two D-D reactions is about 50%. Ignoring escape of the

tritium, the production rate of the low and high energy neutrons is the same. Some of the tritium, however, escapes from the plasma before being consumed in the D-T reaction. The escape probability depends on the confinement relative to the $\langle \sigma v \rangle_f$ for D-T. In subignited, driven systems the escape probability can be significant.

The performance of NET with D-^{3}He fuel can be calculated using power balance considerations to get the fusion power produced and the losses from the plasma. The loss mechanisms of concern are radiation losses by bremsstrahlung and synchrotron radiation, and transport across the confining magnetic field by conduction and convection. The plasma density and temperature that can be confined by the magnetic field are determined by MHD equilibrium and stability requirements. The plasma pressure, which is of concern for MHD, is determined not only by the fuel plasma, but also by the energetic ions generated by fusion reactions, and by the accumulation of ash and impurities. The energy of the charged particles generated by the fusion reactions also helps to maintain the energy of the reacting plasma. Folding all these effects together provides a mechanism for estimating the performance of NET using D-^{3}He fuel.

A computer code, called DHE3TOK, has been developed in order to estimate the performance of a NET-like tokamak operating with D-^{3}He. The basic physics assumptions built into this code are the same as one uses in the DT version of NET. We have used in the code the same level of conservatism or optimism as is implied in the analysis of NET by the NET design team. In particular, the following assumptions are made:

1. The beta, ratio of plasma pressure to magnetic pressure, is determined by the Troyon formula, which is an empirical fit to numerical MHD calculations.
2. The energy confinement time is given by empirical scalings.

The code is basically a zero-dimensional power balance code which calculates the ignition margin, M, defined as the ratio of the fusion power produced to the total losses, and the energy multiplication, Q, which is defined as the ratio of the fusion power to the power injected into the plasma, for a given set of plasma conditions. The injected power is the power required to sustain the plasma conditions. Note that Q = 1 (breakeven) in a D-^{3}He plasma is a

stronger condition than Q = 1 in D-T because in the D-T case 80% of the power produced is in the form of neutron energy. The Q = .2 case in D-^{3}He is equivalent to Q = 1 in D-T from the impact on the plasma power balance and the study of burn physics.

The plasma contains two fuel ion species (deuterium and ^{3}He) and three "ash" ion species (protons, alphas, and tritium). We also allow for a single impurity ion (e.g. oxygen), which is assumed to be fully stripped. Protons and alphas are produced primarily by the ^{3}He(d,p)^{4}He reaction. The D(d,p)T side reaction produces tritium which is important for evaluating the generation of 14 MeV neutrons. The density profile of each charged particle species is taken to be parabolic. The electron and ion temperature profits are taken to parabolic raised to the 1.5 power.

The fusion power, P_f, is given by integrating the local fusion power density over the plasma. This calculation involves the Maxwellian-averaged fusion cross-section $\langle\sigma v\rangle_f$, which depends on r through its dependence on the ion temperature and assumes the two ion species are Maxwellian at the same temperature. We include the accumulation of fusion produced ash (protons, tritons, and alpha particles); the ash density is determined by the balance of the production rate and the loss rate. The particle confinement time is taken to be the same for all species. The electron density is determined by quasineutrality.

The volume averaged plasma beta is given by the Troyon formula [7],

$$\langle\beta\rangle = \frac{C\ I_p\ (MA)}{a(m)\ B_0(T)}$$

where I_p is the plasma current, B_0 is the magnetic field on axis and a is the plasma half width. This equation requires that the quantities be entered in the units indicated. The NET team has used the value C = .035; we use the same value for this study. Included in the pressure are the effects of the various ion species, all of which are assumed to have the same ion temperature, the electrons, which have temperature $T_e(r)$, and also the pressure [8] of the hot ions generated by fusion reactions.

To determine the injected power required to sustain the plasma at a specified operating temperature, it is necessary to account for the various mechanisms by which the plasma loses energy. Bremsstrahlung radiation, with

relativistic corrections [9], from the electrons is an important loss process, especially at low temperature and high density.

Synchrotron radiation from the electrons is another form of radiation loss. While this is a classical process and is in principle calculable, it is a difficult radiation transport problem because the plasma is both a strong emitter and absorber of synchrotron radiation. We use a "universal formula" developed by Trubnikov [10] to estimate the synchrotron power loss.

The reflectivity of the first wall is a concern. IPP Garching provided steel plates which had been exposed to plasma in the ASDEX divertor chamber. The JET team provided graphite tiles which were exposed to plasma in the JET tokamak. The reflectivity of the steel plates and graphite tiles was measured by G. Hochschild and H. Stickel of KfK. This yielded an average reflectivity of .95. It was assumed that 20% of the first wall surface is holes. Consequently, an effective reflectivity of .77 for synchrotron radiation was used in this study.

The remaining energy loss process is transport across the magnetic field by conduction and convection. This is treated using empirical energy confinement times. The NET team has used the ASDEX H-mode confinement time [6],

$$\tau_H = .1\ I_p\ (\text{MA})\ R\ (\text{m}) \qquad (\text{s})$$

which is based on H-mode operation in the ASDEX tokamak. There are a variety of alternative "scaling laws" for energy confinement. An often used scaling law is the Kaye-Goldston [11] scaling law,

$$\tau_{KG} \propto I_p^{1.24}\ P_{ext}^{-.58}\ R^{1.65}\ a^{-.49}\ K^{.28}\ n_e^{.26}\ A_i^{.5}\ B_0^{-.09}\ f_H$$

where A_i is the atomic mass number of the ions. This scaling law is determined empirically from a larger set of data covering many tokamaks operating in the L-mode regime with sufficient auxiliary heating. To account for the improved confinement in the H-mode regime, the factor f_H is introduced. One normally takes f_H to be 2. The heating power, P_{ext}, is taken to include the fusion power as well as the actual external power.

The transport energy loss is primarily due to the electrons in present experiments. The ion energy transport has generally been assumed to be within a factor of 2 or 3 of the neoclassical energy transport, although more recent

results have called this into question. At the conditions appropriate for D-^{3}He the neoclassical energy confinement time for the ions is very long in comparison with the empirical energy confinement times given above. The energy flow for the system is as follows: The fast ions produced by fusion reactions slow down in the plasma and transfer their energy to the background ions and electrons; the electrons get the larger share in a D-^{3}He plasma (about 80%). The fuel ions are also heated by the external heating system, if present, and lose energy to the electrons by Coulomb collisions. Because the energy flow has to be from the ions to the electrons, the ions are hotter than the electrons. The electrons radiate some of the power to the walls and transport the rest by thermal conduction across the magnetic field. Some of the external heating power may also be coupled to the electrons depending on the heating mechanism chosen. In this report, we assume that, with suitable design of an ICRF system, the power can be coupled only to the ions and neglect any coupling to the electrons. If the plasma is ignited then the external heating power is zero and the radiation power must be increased to maintain a power balance.

We now present the results of parametric studies using the above model. We first consider the NET-DT and NET-EP tokamaks with no changes in the dimensions or magnetic field, but change only the fuel composition from D-T to D-^{3}He and change the operating temperature to that required for D-^{3}He, with a corresponding change in the injected power because of the higher operating temperature.

Shown in Fig. 4 is the Q-value that can be obtained in the reference NET-DT tokamak for the two scaling laws, Kaye-Goldston and ASDEX H-mode, versus the average ion temperature. We see that the optimum ion temperature (all temperatures quoted in this section are density weighted and averaged over the plasma volume) is about 45 keV. It is obvious from Fig. 4 that the plasma performance is much more favorable for ASDEX scaling than for Kaye Goldston scaling. It is gratifying to note that $Q \tilde{=} 1$ could be achieved in the NET device as it is presently designed with essentially no modifications (or added cost).

Shown in Fig. 5 is the injected power required to maintain the plasma at the operating temperature and the resulting fusion power; the injected power decreases with increasing ion temperature for ASDEX H-mode scaling since the beta is kept constant at the Troyon limit. Hence density is decreasing as the

temperature is raised in Fig. 4 and 5. The power levels required are excessive if the confinement is Kaye-Goldston, but within the present NET limits if the confinement is ASDEX H-mode. Note that this power is the power coupled to the plasma since the details of the heating mechanism, and hence the coupling efficiency are beyond the scope of this study. (The NET design calls for 50 MW of coupled power for plasma startup and heating to ignition.)

Shown also in Fig. 5 is the fusion power released versus ion temperature. The relatively low fusion power obtained is of concern since the fusion power density is low in the plasma. Consequently, the plasma will be sensitive to impurity accumulation which, in turn, affects the fusion power and the Q-values.

Shown in Fig. 6 is the Q-value obtained with the NET-EP configuration. The injected power and the fusion power versus ion temperature are shown in Fig. 7. We see that with ASDEX H-mode scaling a Q value of 1.45 is obtainable with an injection power of slightly less than 40 MW. With Kaye-Goldston scaling the maximum Q-value is less than .5 and the required injection power is almost 170 MW. Consequently, if the ASDEX H-mode scaling law holds, one can achieve breakeven in NET-EP with no change in the basic machine parameters except for the fuel composition and the operating temperature. There will need to be some modifications to the auxiliary heating system because of the change in fuel and operation temperature.

The NET-DT and NET-EP reference designs have a large region for a thick tritium breeding blanket and shield between the plasma and the TF magnet. This is not needed for D-^{3}He operation. The blanket can be removed and the shield replaced by a thinner shield optimized for the D-^{3}He neutron spectrum. Consequently, the plasma major radius can be reduced; this leads to a lower plasma aspect ratio, higher beta, and higher plasma current if the MHD safety factor is held constant. The higher plasma current increases the energy confinement time. In addition, the reduced major radius of the plasma increases the magnetic field at the plasma and increases the fusion power output. All this is accomplished with the original TF coil design and operating conditions.

Shown in Fig. 8 is the effect of reducing the major plasma radius on the Q-value and the plasma current. In this figure the average ion temperature is kept constant at 37 keV. The Q-value reaches a value of about 2.9 for ASDEX H-mode scaling and the plasma current increases from 14.8 to 20 MA when

the plasma radius is reduced from 5.41 m to 4.61 m. The required injection power decreases slightly from 40 MW to 35 MW. For Kaye-Goldston scaling, the ignition margin increases to .74 and the injection power to 180 MW when the major radius is reduced to 4.61 m.

At a major radius of 4.61 m, the space available for the shield, cryostat, and inboard scrape-off layer has been reduced to a total of 45 cm. Because of the greatly reduced neutron wall loading (0.019 MW/m^2), the magnet can still be protected adequately against nuclear heating and radiation damage effects. The value f_d (deuterium fraction in the fuel) = .65 used so far has been chosen to optimize the Q-value. Reducing the percentage of deuterium in the fuel will reduce the D-D reactions and the production of tritium. Shown in Fig. 9 is the effect of f_d on the Q-value and the amount of power in D-T and D-D neutrons. This graph corresponds to the R = 4.61 m point in Fig. 8. We see that f_d = .65 is about the optimum fuel mixture and Q drops sharply as the deuterium fraction is increased or reduced.

It is worthwhile to consider the relative magnitude of the various loss terms to see the sensitivity of a possible operating point to uncertainty in the various loss terms. Shown in Fig. 10 is the power in the various loss mechanisms normalized to the fusion power versus ion temperature. This curve is for the R = 4.61 m, f_d = .65 case. We see that in the temperature range where Q is largest ($\langle T_i \rangle$ = 35 to 50 keV) transport is the largest single loss; synchrotron is next and bremsstrahlung is close behind. We see that bremsstrahlung dominates at low T_i, but drops rapidly as T_i increases; this is because the density is high when the temperature is low. Consequently, the Q-values given in this report are rather sensitive to uncertainties in the energy confinement time scaling laws.

The above calculations are based on the ASDEX H-mode scaling law for energy confinement. With Kaye-Goldston scaling and an H-mode factor of 2.5, breakeven (Q = 1) can be achieved with a major radius of 4.61 m. The required injection power is about 130 MW; this is a rather large amount of power in comparison with the 50 MW planned for NET and would require 100-200 million dollars in heating equipment.

A second option for improving the performance of NET-EP with D-^{3}He is to increase the magnetic field strength without changing the plasma dimensions. This regime does not benefit from the reduced aspect ratio obtained with the reduction of major plasma radius, but it has a lesser impact on the poloidal

field magnet system since the plasma position is not changed. Shown in Fig. 11 is the Q-value and the plasma current versus maximum magnetic field strength at the TF magnet. This figure uses ASDEX H-mode scaling with the mean ion temperature held at 50 keV. As expected, we see that increases in the magnetic field strength also increase Q and the current. Comparing Figs. 8 and 11, we see that increasing B_c gives more increase in Q for the same increase in plasma current than reducing the plasma radius. Consequently, if the increased plasma current is a major concern, it may be better to get to high Q by increasing B_c at constant R, rather than reducing R at constant B_c.

Finally, we consider the possibility of achieving ignition in a D-^{3}He plasma. To achieve ignition with ASDEX H-mode scaling, it appears necessary to both reduce the major radius and aspect ratio, and to increase the magnetic field at the TF coil. In addition, one can consider raising the plasma elongation; this affects both the beta and the confinement since it raises the plasma current. Shown in Fig. 12 is the elongation required for ignition versus magnetic field strength at the TF magnet. The major plasma radius is held constant at 4.61 m and the plasma half-width is 1.69 m. It is somewhat surprising that the plasma current is essentially constant at about 29 MA along the curve in Fig. 12. This is probably due to strong coupling between plasma current, energy confinement, and beta. The range of plasma elongations shown in Fig. 2.3-11 is above the value (κ = 2.2) considered to be the limit from a MHD point of view. The higher magnetic field strength (13 T) is not considered to be feasible within the context of the guidelines used for the NET toroidal field magnet design. Because of these limitations, ignition in NET is not likely.

So far we have considered parameters where substantial changes to the inboard shield and/or TF magnets are required. While the impact of these changes on the total cost of NET is small, nevertheless these changes can have an adverse effect of the operation schedule of NET since the shield for D-^{3}He operation will have to be replaced with that required for D-T operation. It is worthwhile to consider in more detail D-^{3}He operation using the D-T shield. The inboard blanket is assumed to be left out during the D-^{3}He phase and protective tiles are installed on the face of the steel D-T shield. Postponing the installation of the inboard blanket to after the end of the D-^{3}He phase of operation allows the plasma major radius to be reduced by 27 cm. We now

consider the Q-value that can be achieved with this configuration, referred to as case A-3 in later discussion. We also consider the effect of impurity and ash accumulation on the Q-value achieved. The impurity is assumed to be oxygen and is given as a percentage of the total fuel ion density. Raising the concentration from zero to 2% decreases Q from 1.6 to 1.0. In this calculation, the impurity affects the plasma through the increase of the electron concentration (required for quasi-neutrality) and the corresponding reduction of the fuel density for a given β. The synchrotron and bremsstrahlung radiation losses are also increased but the impurity ions are assumed to be fully stripped so that there is no line radiation from the impurity ions.

Another poorly known factor is particle confinement. Particle confinement affects the power balance through the accumulation of ash in the plasma. Assuming ASDEX H-mode scaling and a 1% oxygen impurity, increasing τ_p reduces Q from 1.26 at $\tau_p/\tau_E = 1$ to .96 at $\tau_p/\tau_E = 10$. The current understanding is that τ_p/τ_E is about 3 in the steady state for present discharges, but the effective τ_p is much less than τ_E in transients; this difference is because of the pinch effect playing a role in the steady state transport. We can tolerate a combined effect of 1% oxygen content and $\tau_p/\tau_E = 3$ and still achieve $Q = 1.2$ in this mildly revised NET configuration. With no impurities and $\tau_p/\tau_E = 1$, $Q = 1.6$, so the loss in Q is about 25%.

The operating space for case A-3 is shown in Fig. 13 for ASDEX H-mode scaling. This figure shows the injection power required to achieve a given average ion density and ion temperature; the electron temperature is calculated self-consistently. Also shown in the figure is the Q-value obtained at those plasma parameters. One can see the reduction in Q caused by having less power available. This figure also illustrates the path to take in this density - temperature space during startup to minimize the required injection power to achieve a desired operating point. We see that startup of the plasma does not require more power than that required to sustain the plasma at the final operating point. This is a feature of driven systems with Q less than or near unity. Figure 14 shows the operating space for case A-3, but with Kaye-Goldston energy confinement scaling and an H-mode factor of 2. In this case, the power required to sustain the plasma at the beta-limit is rather large, about 175 MW. At this point $Q = .47$. Reduction of the injected power to 80 MW yields a maximum Q-value of .2.

The major parameters for possible operating points are given in Table II. Case A-1 is the reference NET-DT design and case A-2 is NET-EP. Case A-3 is NET-EP with the major radius reduced by 27 cm and 1% oxygen impurity content. In this case $\tau_p = 4\ \tau_E$, whereas $\tau_p = \tau_E$ in all other cases. Cases B-1 and B-2 are reduced major radius cases with different fuel composition. Case C-1 is the same size as A-2, but with increased toroidal field. Cases D-1 and D-2 represent possible ignition cases.

The above predictions are obtained using the ASDEX H-mode scaling law. Breakeven in NET is possible with the Kaye-Goldston scaling law for an H-mode factor of about 2.5, but the required injection power is about 120 MW. This assumes the major radius of the plasma has been reduced to 4.61 m and the toroidal field at the magnet remains at the NET value of 10.4 T.

From these results we see that significant energy multiplication in a mildly revised form of NET can be obtained if nature is not too perverse. Significant energy multiplication means that the fusion reactions are as important as the external heating power in determining the power balance of the plasma. Consequently, important questions regarding burn physics and the effects of a significant number of fast fusion produced ions in the plasma can be studied with such a machine. In addition, the much reduced neutron production makes the environment more hospitable to performing physics experiments on burning plasmas than is the case with DT fuel.

3. NEUTRONICS

The goal of the neutronics analyses is to determine the radiation level at the TF magnets. The analyses were carried out for two cases; the first part of the analysis is applicable to cases B and D of the parametric studies. The second part of the analysis pertains to case A-3 where the breeding blanket is removed and the permanent shield is left in place. The NET device is a low fluence machine. It is expected to be designed for 1000 shots with a shot duration of 200 seconds. A machine lifetime of 2×10^5 s is anticipated, which is equivalent to 2.32 full power days (FPD). The total nuclear heating in the 16 TF coils is limited to 20 kW. The limits on the dose to the GFF epoxy and fast neutron fluence ($E_n > 0.1$ MeV) are taken to be 5×10^8 rads and 5×10^{17} n/cm^2, respectively.

Shielding Analysis for Cases B and D

The objective of this analysis is to design the thinnest possible inboard shield that satisfies the TF magnet radiation limits and engineering constraints, for cases B or D. The minimum shield thickness is desired since, for a given magnetic field at the TF magnets, increasing the shield thickness moves the plasma to larger radius and therefore a lower magnetic field. This reduces the fusion power and Q. The primary shield design requirement is to limit the TF coil nuclear heating to 20 kW. The engineering constraints are that the geometry of the TF coils and the dimensions of specific regions (such as the cryostat, gaps, and scrape-off) remain the same as that of the NET-DT design.

In the NET-D^{3}He design, the breeding blanket of the NET-DT design was removed, the outboard permanent shield was left in place, and the inboard shie d was thinned to accommodate the larger plasma size. The NEWLIT code [12] was used to determine the poloidal variation of the neutron wall loading; the results of the calculations are given in Fig. 15. The first wall and plasma shapes are shown, as are the magnetic flux surfaces. The wall loading distribution in each segment is indicated and the dashed line represents the average neutron wall loading. This figure is generated for case B-1 with inboard scrape-off thickness of 6 cm and a deuterium fraction of 0.65.

The highest damage in the inner legs of the TF coils occurs at the midplane of the reactor where the neutron wall loading has its peak value. The winding pack composition is taken as 34.5 v/o 304 SS, 33.4 v/o Cu, 3 v/o Ni, 6.6 v/o Nb_3Sn, 11.7 v/o GFF epoxy, and 10.8 v/o liquid helium. There is a 5.5 cm thick cryostat and a 1.5 cm gap between the cryostat and the back of the shield.

An optimization study was performed to determine the optimum shield composition that minimizes the nuclear heating in the magnets. Tungsten alloy is used as the main inboard shielding material to provide adequate protection for the inner leg of the magnet. The coolant is borated water (5 g boric acid/100 cm^3 of H_2O) and the structure is PCA. Two additional shielding materials were considered at the back of the W-shield. These are B_4C (at 90% density factor and 90% ^{10}B in B) and Pb. The outboard shield was taken as 90 v/o PCA and 10 v/o coolant. The inboard shield consists of alternate layers with a thick W-shield followed by a B_4C-shield and then a Pb-shield. In all layers, we considered 10 v/o structure and 5 v/o coolant. In the

optimization study, the three layers were varied in thickness to reduce the nuclear heating in the magnets. The optimum shield was found to consist of 77.3% W-shield, 14.7% B_4C-shield, and 8% Pb-shield by thickness.

The radiation effects at the TF coil are given in Table III for a total shield thickness of 29 cm and an inboard scrape-off layer of 6 cm. The peak values occur at the midplane of the inner legs. The dose to the GFF epoxy and the fast neutron fluence are much below the design limits. In addition, the end-of-life radiation-induced resistivity in the stabilizer is less than ~ 1% of the unirradiated stabilizer resistivity at the operating field. The nuclear heating in the TF coils is less than the 20 kW limit. This suggests that the shield can be made thinner in order to meet the heating limit.

Figure 16 shows the variation of the heating in the magnets as a function of the shield thickness for different f_D values and scrape-off layer thicknesses. The drop in the heating rate in the scrape-off layer thickness is increased due to the lower neutron wall loading as a result of the farther plasma location and the lower neutron power. The variation also shows that the total heating increases by a factor of 2 for each 4 cm decrease in the shield thickness. Therefore, to meet the heating limit, the inboard shield can be as thin as 27, 23, and 16 cm for f_D values of 0.65, 0.5, and 0.3, respectively.

Shielding Analysis for Case A-3

In case A-3, the tritium breeding blanket of the NET-DT design was removed and the only shield left in place is the permanent shield. The permanent shield (which acts also as a vacuum vessel) developed by the NET team is 70 cm thick on the inboard side and 59 cm thick on the outboard. It is cooled with borated water (4 g of boric acid/100 cm^3 of H_2O) and composed of two layers of steel shield.

Compared to regime B and D, case A-3 is not expected to have any shielding problem. For a deuterium fraction of 0.65, the neutron power is 7.8 MW. The neutron wall loading distribution for case A-3 was generated using the NEWLIT code. The wall loading peaks at the midplane of the inboard side with a value of 0.0155 MW/m^2. The average wall loading is 0.01 MW/m^2 and the outboard peak is 0.0145 MW/m^2. The results are listed in Table III. The peak values occur at the midplane of the reactor where the wall loading maximizes. The outer legs have higher damage due to the difference in the material arrangement. The total nuclear heating in the 16 TF coils is estimated to

be ~ 0.6 kW in the winding packs and ~ 0.8 kW in the coil cases of the outer legs. The other radiation effects are much below their design limits.

4. FAST ION EFFECTS

The loss of fast ions to the first wall is potentially a more serious problem in D-^{3}He tokamaks than in D-T tokamaks. This is because almost all the fusion energy is produced in the form of energetic charged particles, rather than 20% as in D-T. Furthermore, 80% of the fusion energy is carried by the 14.7 MeV protons, which have twice the gyroradius of the 3.5 MeV alpha particles produced in a D-T reactor. Consequently, the fast protons are more susceptible to finite orbit effects and trapping in the magnetic field ripple. These effects lead to transport of the fast ions to the first wall. A small fraction of the fast protons can be born on orbits which intersect the first wall; this loss mechanism is small, even in tokamaks the size of NET, and becomes insignificant in reactor-sized tokamaks. More serious is the possibility of fast ions becoming trapped in the toroidal field magnetic ripple and drifitng to the first wall before slowing down to thermal energies. This problem is an active area of research [13-15] for D-T tokamaks (there is still no consensus on the severity of the problem for a particular set of machine parameters), and is basically unassessed in D-^{3}He tokamaks.

5. PLASMA REFUELLING

We consider next the possibilities of pellet injection, neutral beam injection, and plasma injection for refuelling a NET-like tokamak operating on D-^{3}He.

Pellet Fuelling

Pellet fuelling a D-^{3}He plasma differs from fuelling a D-T plasma in two respects. First is the question of how one makes a pellet containing ^{3}He, which does not solidify unless it is pressurized to about 30 atmospheres. Wittenberg [16] has suggested encapsulating liquid ^{3}He in a thin walled polymeric shell which is then overcoated with deuterium. This pellet can then be accelerated using techniques developed for solid deuterium pellets.

The second difference between fuelling a D-3 He plasma and a D-T plasma is the higher electron temperature in the D-^{3}He plasma. This leads to an increased ablation rate by electron bombardment. In addition, the fraction of fast ions is somewhat higher in a D-^{3}He plasma, which also increases the

ablation rate. Using the neutral gas shielding model of Milora and Foster [17] which considers only ablation due to electron heating, we estimate that pellet injection velocities ranging from about 15 km/s to several hundred km/s are required, depending on the penetration depth desired and the fraction of the fuel charge in a single pellet. These injection velocities are excessive for a near term device and hence alternative fuelling schemes are needed.

Pellet fuelling may be useful in controlling the density profile near the edge of the plasma. In this case, the required injection velocity is much less. In addition, the pellets need not contain helium, but can be pure deuterium, since the helium refuelling is needed only in the center where the D-^{3}He fusion reactions occur.

Neutral Beam Refuelling

Neutral beam injection is another possible fuelling mechanism. Since helium does not charge exchange well with hydrogen isotopes, one might think the required injection energy may be considerably less for a helium beam than it is for a deuterium beam. The relevant atomic reactions for a neutral 3He beam penetrating the plasma are electron impact ionization, ion impact ionization with both D+ and He++ ions, charge exchange with D+ and one-electron and two-electron charge exchange with He++. These cross-sections are available only partly available, and then only for ^{4}He. If we assume that the cross-sections depend fundamentally on the relative speed of the interacting particles and that the different mass of the ^{3}He nucleus does not matter, then estimates of the penetration depth of a ^{3}He neutral beam can be made. We find that penetration to the center for the moderate Q cases (A-1, A-2, and A-3) in Table II require an injection energy of about 300 keV.

The next concern is the required injection power; this depends on the beam current which is determined by the particle confinement time in the center of the discharge. If we consider refuelling inside the a/2 flux surface by NBI and assume the particle confinement time is four times the energy confinement time then the required absorbed current in the central zone is 20 A for Case A-2. Allowing for absorption of the beam in the outer regions, the required current at the plasma edge is 32 A equivalent (assuming Z=1). This is 9.6 MW of refuelling beam power, which is small compared with the 37 MW required to drive the plasma at this operating point.

Helium refuelling of the outer half of the plasma is not really required. A reduction of the helium content in the annular region $a/2<r<a$ does not cause

a significant loss of fusion power, because the power density is proportional to $n^2\langle\sigma v\rangle_f$, which is localized to the center through the spatial dependence of $n(r)$ and $T_i(r)$.

Applying the same analysis to the refuelling of deuterium by NBI, we find that 3000 keV is required for injection to the center. For central refuelling, the required beam current is 60 A equivalent and the beam power is 18 MW. Refuelling the outer half of the plasma with deuterium requires a 28 MW, 60 keV NBI system, if we assume the "edge" τ_p equals τ_E. The total NBI power for both helium and deuterium refuelling would be 56 MW, which is above the 37 MW required to sustain the plasma. The additional 19 MW could be considered as a safety factor for impurities and other losses.

Not included in this analysis is the very outer edge of the plasma where the recycling is high. This region refuels itself through recycling processes in the divertor and scrape-off layer.

Plasma Injection

Refuelling by plasma injection is an old idea [18,19] that has been revived recently for refuelling of tokamaks. There are two basic ideas for plasma injection. The first, and oldest, is injection of plasma from a Marshall gun or other suitable source which crosses the external magnetic field by polarization electric fields. The second is the formation and acceleration of compact toroid plasmas which have a very high energy density and cross the magnetic field by "punching" a hole in the field.

It is well-known [20] that a moving plasma can cross a vacuum magnetic field provided it meets the condition $\omega_{pi}^2/\omega_{ci}^2 \gg 1$, where ω_{pi} and ω_{ci} are the ion plasma and ion cyclotron frequencies, respectively. As the plasma moving with velocity $\vec{V}$ encounters a magnetic field, ions are deflected one way and electrons the other way. This creates a polarization electric field, $\vec{E}$, which builds up until $\vec{E} = -\vec{V} \times \vec{B}$. At this point the interior of the plasma beam can move across the magnetic field with its original velocity $\vec{V} = \vec{E} \times \vec{B}/B^2$. In this situation there is no electric field in the frame of reference moving with the plasma beam and hence no current flow. The stopping of such a plasma beam has to be done by shorting out the polarization electric field [21].

Tokamaks have both toroidal and poloidal magnetic fields with a spatially changing rotational transform. The depolarization process required for deceleration can occur by finite resistivity and an $\vec{E}$ parallel to the motion

and produce stopping of the plasma stream. In addition, the plasma stream is injected into a torus already containing a well-formed tokamak plasma with very low resistivity because of its high electron temperature. An additional depolarization possibility is the flow of current along the magnetic field in the external plasma which can short out the polarization electric field. These processes require evaluation to assess the suitability of refuelling by this means.

Refuelling of a tokamak by gun injection has been accomplished successfully in the Tokapole II experiment [22,23]. In this experiment involving a small tokamak (major radius = 50 cm, minor radius = 10 cm, B = 5 kG) the density on axis was increased by about 50% in a single shot from a Marshall gun. The theoretical model developed for this experiment was based on current flowing radially across the magnetic field by the electric field produced by the changing pitch angle of the magnetic field. A detailed quantitative comparison with the experiment was not possible, but the model gave estimates for the stopping length in reasonable agreement with the data and also predicted qualitatively the observed scaling of the trapping with plasma current and toroidal magnetic field.

Plasma contamination due to gun injection is always a concern since gun plasmas have the reputation of being "dirty". In this regard it is important to note that the gun plasma did not noticeably increase the impurity content of the Tokapole discharge. If this were a problem, then alternative plasma sources which don't involve drawing a current between electrodes could be developed.

Applying the model developed for the Tokapole experiments to refuelling of NET with D-^{3}He gives one assessment of the possibility of refuelling of NET using gun injection. If we assume the gun produces a plasma with a density of 10^{16} cm^{-3} with $T_e \sim 10$ eV, a velocity of 10^7 cm/s, a beam radius of 25 cm and a beam length of 1 m, then the stopping distance predicted by the model is 5 m. This is more than adequate to insure penetration to the center and longer than desired since the plasma half-width in the horizontal midplane is 1.7 m. Each refuelling shot introduces a fuel charge which is about 6% of the fuel present in the discharge; hence the density fluctuation with each shot is only about 6%. To maintain the fuel density, a repetition rate of 1 shot every 1.5 s is required. This can be provided by a number of refuelling guns firing less frequently.

A possible competing process for shorting out the polarization electric field is current flow through the external plasma along the magnetic field. Because the MHD safety factor is about 2, a field line connects the top of the plasma stream, where the polarization charge density has one sign, to the bottom, where the charge density has the opposite sign, after one transit around the torus. It is important to note, however, that this current path has a high inductance and, consequently, the pulse time of the plasma beam entering the discharge is important in determining the impedance of this current path. For the Tokapole discharge this impedance was estimated to be too large for this effect to be significant. Applying this deceleration process to refuelling of NET, using the parameters mentioned earlier, gives a stopping distance of 100 cm, which is about what is needed for adequate penetration to the magnetic axis. For NET with D-^{3}He parameters, it appears that this depolarization process is more important than the one apparently involved in the Tokapole II experiment.

Compact Toroid Injection

Refuelling of tokamaks by the injection of plasma in the form of compact toroids has been proposed [24]. The compact toroid injectors offer very high injection velocities with a sizable amount of plasma injected per shot. Compact toroids with a mass of .5 mg have been accelerated to about 400 km/s in the RACE experiments at LLNL, while velocities over 2500 km/s have been achieved [25]. The lifetime of the compact toroid can be greater than a millisecond, depending on the electron temperature; this allows adequate time for acceleration of the plasma to high velocity. These results are very encouraging for the refuelling of large tokamak plasmas. Furthermore, the compact toroid should be insensitive to the nuclear composition of the plasma of which it is composed and should therefore be suitable for injecting a D-^{3}He fuel mixture.

The compact toroid refuelling scheme considered for TIBER [26] is applicable to D-^{3}He refuelling in NET because the slowing down and tilting of the compact toroid is determined by the toroidal field of the tokamak and not by the properties of the tokamak plasma. The NET device is somewhat larger, but this is compensated by the higher toroidal field, and field gradient, in TIBER. Consequently, the interaction and refuelling properties of the compact toroids should be pretty much the same.

The proposed compact toroid fuel injector for TIBER used an injection velocity of 750 km/s with an injected mass per shot of 5 mg and a repetition rate of .9 Hz. The estimated time-averaged "wall-plug power" for refuelling was 2.5 MW, which is low considering the output of the plant. This system could be used on a D-^{3}He NET without any major changes. Because of the lower ion density in a D-^{3}He NET, compared with TIBER, the Alfvén velocity is higher. Consequently, the injection velocity could be increased if this were desirable. The estimated capital cost of the compact toroid injector system for TIBER was 15 million dollars. It should also be noted that the same system can be used for refuelling both D-^{3}He experiments and D-T experiments.

6. ICRF HEATING

We examine ICRF D-^{3}He heating and fusion scenarios for the NET Enhanced Physics (NET-EP) and NET A-3 cases. Issues include: 1) the single pass NET-EP and NET A-3 minority ^{3}He and second harmonic absorption at concentrations ranging from 2-25%, 2) deuterium and fusion proton ICRF absorption in the machine and 3) the fusion Q factor in the subignited state when compared to the Q for Maxwellian distributions.

The concept of ICRF enhanced fusion Q (fusion power out/auxiliary power in) was first examined by Scharer, Jacquinot, Lallia and Sand [27] for a modest ICRF power level near breakeven for D-T operation in JET. It was found that minority deuterium fundamental ion resonance non-Maxwellian tail heating produced fusion Q enhancements of factors of two compared to a Maxwellian equivalent. Majority deuterium second harmonic heating was also found to produce Q enhancements for D-T reactors by the same order of magnitude by Harvey, Kerbel and McCoy [28]. In recent JET [29] and earlier PLT [30] D-^{3}He ICRF ^{3}He minority ion heating experiments 3-5 keV majority deuterium ion temperatures have been achieved with strong tail formation. The γ-ray detection measurements on JET [31] have inferred 9 kW of D-^{3}He fusion power and a $Q = P_{fusion}/P_{RF} = 2 \times 10^{-3}$. Current experiments underway planned for up to 20 MW of ICRF power anticipate a good fraction of a megawatt of D-^{3}He fusion power and a fusion Q of several percent.

Single Pass Fast Wave Absorption for NET-EP and NET (A-3 case) D-^{3}He Plasmas

To examine the efficiency of absorption for NET-EP parameters we use a computer code corresponding to a definition of power absorption and the associated conservation relation for inhomogeneous plasmas developed by McVey,

Sund and Scharer [32]. The code correctly solves the propagation and coupling of incident fast magnetosonic waves from the low field side of the machine to ion Bernstein waves in the resonant core region. It has also been checked with good agreement with a PLT data set and range of parallel wavelengths with other groups at Princeton, ORNL and NYU.

We take parameters corresponding to startup with a 7 keV temperature for all species with an electron density of $1.78 \times 10^{14}/cm^3$, a toroidal field on axis of 5.6 T and a minor radius of 1.7 m. The helium fraction is taken to be 2% initially to achieve an optimum single pass absorption at lower temperatures. Figure 17 shows the dispersion relation near the core helium resonance for the incident and reflected fast wave (F) at a frequency of 115 MHz and incoming and outgoing Bernstein (B) wave, which is a backward wave in a tokamak. The solid lines correspond to the real part of the wavenumber and the dashed lines correspond to the imaginary parts which indicate absorption or mode conversion.

The real and imaginary parts of the left hand polarization of the composite field solution are shown on Fig. 18. Note the peaking of this heating component on the high field side near resonance at $x = 0$. Finally, the local absorbed power and Poynting and kinetic flux for the incoming wave are shown in Fig. 19. The electron absorption is a small part of the heating (7%) corresponding to the cross-hatched region with the majority of the 65% single pass total absorption done by the helium species. The production of ion tails should broaden this absorption curve and increase the single pass absorption values.

The previous case, which has a very low helium concentration of 2%, achieves good single pass absorption at lower startup temperatures. As the plasma heats up, the helium concentration can be raised to 35% although an absorption description at elevated temperatures $T_{eff} \simeq 50$ keV at this high density is more complex. An alternative heating scenario uses second harmonic helium absorption at a frequency of 230 MHz. This would make the single pass absorption less sensitive to the helium concentration but would yield a lower single pass absorption and reactivity enhancement during startup.

Next we consider case A-3 with $n_{He}/n_e = 15\%$. At a frequency corresponding to the helium fundamental at the core and a $k_{\parallel} = 8\ m^{-1}$ we obtain 87% helium and 12% electron absorption in the 20 cm core region at an ion temperature of 80 keV. If the ion temperature is 40 keV with 33% of the helium

distribution having a tail temperature of 200 keV and all other parameters the same, then 50% of the fast wave incident power goes to the bulk helium ions and 29% to the tails with 19% going to the electrons. This means that a radiofrequency generator set designed for fundamental minority helium absorption in a D-T plasma could provide reasonable absorption at these higher concentrations when the plasma temperature is increased.

At still higher concentrations of helium, the fundamental absorption degrades but the second harmonic absorption on the helium-3 is quite efficient. At a helium concentration of 25% and 50% deuterium with 10 keV plasma temperatures and a $k_{\parallel} = 8\ m^{-1}$, the helium second harmonic single pass absorption is 85% with a 7% electron absorption. At more elevated ion temperatures of 50 keV with 40 keV electrons and 25% helium concentrations, a parallel wavelength of $k_{\parallel} = 4\ m^{-1}$ yields 75% absorption by the helium and 25% by the electrons in the 20 cm core.

7. HEAT LOADS ON THE FIRST WALL AND DIVERTOR

The heat load on the first wall is composed primarily of three parts. First, there is the load from synchrotron and bremsstrahlung radiation emitted by the plasma. Next, there will be a neutral particle flux incident on the first wall. Finally, there will be energetic ions striking the wall because of finite orbit effects and trapping in the magnetic field ripple.

For D-^{3}He operation in NET, the average surface heat load due to radiation is not large. For NET-DT and NET-EP the average heat load is about 5 W/cm^2. The Q = 2.5 - 3 cases have an average surface heat load of about 15 W/cm^2, and the ignition cases have an average surface heat load of 30-50 W/cm^2, depending on the plasma elongation. These values are shown in Table II and Table V.

The poloidal variation of the heat load due to bremsstrahlung should have a profile similar to that of the neutron wall loading since, for both forms of radiation, the plasma acts like a volume emitter. The poloidal variation of synchrotron radiation is a little harder to deduce since the plasma is optically thick. Consequently, one expects the escaping photons to have come from near the surface of the plasma. Due to the variation of the magnetic field strength, one might expect the radiation to be stronger on the inboard side where B is higher, since the radiation is proportional to $B^{2.5}$. If we assume the bremsstrahlung radiation has the same poloidal variation as the neutron

wall loading and the synchrotron radiation varies poloidally as $B^{2.5}$, where B is the magnetic field strength at the edge of the plasma, then the inboard and outboard peaks in the first wall heat flux can be estimated. The results are shown in Table V. We see that the peak heat flux occurs on the inboard side and is less than 20 W/cm^2 for cases A-1, A-2, and A-3. The present NET-DT design value for the total peak heat flux on the first wall is 40 W/cm^2 and is set by the stainless steel-graphite design concept. We see that the A cases leave an allowance of at least 20 W/cm^2 and cases B-1 and C-1 are acceptable by this criteria. Cases B-2, D-1, and D-2 exceed this criteria and would require a different design concept. The peak heat flux on the outboard side is considerably less than 40 W/cm^2, except for case D-2. These estimates for the peak heat flux are conservative since synchrotron radiation transport in the vacuum chamber will reduce somewhat the peaking from that used in this analysis. Furthermore, the heat flux here has been calculated using the plasma surface area, and not the true wall area, since the location of the wall is not determined in all cases.

The above estimates do not include fast ion losses, which is a poorly determined loss and depends sensitively on the magnetic field ripple. The fast ion loss is expected to impinge on the wall on the outboard side, where the heat flux is much less than that on the inboard side. Furthermore, the fast ion heat flux is sensitive to the location and shape of the first wall on the outboard side. One can use Table V as an indication of what fast ion heat flux can be tolerated within a given design concept.

An upper limit to the heat load to the divertor is the total fusion power plus the injected power minus the power carried to the first wall by synchrotron and bremsstrahlung radiation. For the NET-DT and NET-EP cases with D-^{3}He, this power is about 55-60 MW. For the Q = 2.5 - 3 cases, this power is about 75 MW, and for ignition it is about 95 - 100 MW. This number should be compared to the alpha heating power of 120 MW in NET using D-T. Consequently, one can expect the power to the divertor with D-^{3}He to be less than, or comparable to, that with D-T. The NET-DT divertor is designed for 80 MW (135 MW in NET-EP) using the assumption that the remaining 40 MW (65 MW in NET-EP) is radiated from the scrape-off layer plasma and is distributed over a larger area than the target plates. Plasma transport and recycling in the scrape-off layer and divertor has not been analyzed with D-^{3}He operation, but there is no reason to expect that the plasma scrape-off layer will be thinner

with D-^{3}He than it is with D-T. Consequently, the power density on the divertor target plates will be similar to, or less than, that already designed for in the D-T version of NET. (Note: values in Table V are maximum heat fluxes to the divertor with no allowances for charge exchange or radiation losses.)

8. CONCLUSIONS

From the analysis presented in this paper, the following conclusions may be drawn. Breakeven (Q = 1) may be obtained in the present NET-DT design if ASDEX H-mode scaling is applicable. In addition, the required injection power is less than that planned for startup in NET-DT. If Kaye-Goldston scaling continues to plague tokamaks, then the Q-values obtained are much lower (Q = .4) and the injection power is much higher (P_{inj} = 120 MW). The enhanced plasma size NET case (NET-EP) can achieve a Q-value of about 1.4 using ASDEX H-mode scaling with no changes in the machine parameters except for the fuel and the operating temperature.

The Q-value can be increased in many ways in NET because of the low neutron production with D-^{3}He fuel. Reduction of the major plasma radius to 4.61 m increases the Q-value to about 3. This improvement in Q is due to the increase in magnetic field at the plasma and to the reduced aspect ratio which leads to higher plasma current, energy confinement times, and beta. The reduction in major radius can be achieved by removing the inboard blanket designed for DT operation and using a much thinner shield designed for the low DD and DT neutron exposure.

An alternative approach is to increase the magnetic field at the toroidal field magnets without changing the plasma dimensions from the NET-EP case. Q values of about 2.5 - 3 can be obtained by a 20% increase in the magnetic field strength at the TF coil.

Ignition with D-^{3}He in NET may be obtained if the plasma major radius is reduced in conjunction with an increase in the toroidal field and in the plasma elongation. The required elongation for ignition is about 2.4 at B_c = 13 T and 2.7 at B_c = 10.5 T. (B_c is the toroidal field at the TF magnet.) A 13 T toroidal field magnet is infeasible for NET within the context of the present design guidelines.

The above predictions are obtained using the ASDEX H-mode scaling law. Breakeven in NET is possible with the Kaye-Goldston scaling law for an H-mode factor of about 2.5, but the required injection power is about 120 MW. This

assumes the major radius of the plasma has been reduced to 4.61 m and the toroidal field at the magnet remains at the NET value of 10.4 T.

We have considered in more detail a minor revision to NET-EP. By removing the breeding blanket, but retaining the NET stainless steel shield, the major radius of the plasma can be decreased from 5.41 m to 5.14 m. The NET shield alone gives sufficient neutron attenuation for D-^{3}He operation such that the TF magnet is more than adequately protected. This configuration, referred to as case A-3, has been used for a more detailed study of issues related to D-^{3}He operation.

Using ASDEX H-mode confinement scaling, this case has a Q value of 1.6 if impurities are neglected. With a 1% oxygen impurity concentration and ash accumulation calculated assuming the particle confinement time in the center is four times longer than the energy confinement time, the Q value decreases to about 1.2.

The feasibility of heating a D-^{3}He plasma using ICRF has been investigated for NET-EP and case A-3. At low helium concentrations (n_{He}/n_e = 2-4%) the single pass RF absorption on the helium at the fundamental ion cyclotron frequency is good. This means that the same RF system needed for a D-T plasma with either second harmonic tritium heating or fundamental minority ^{3}He heating would also work in the D-^{3}He plasma at low ^{3}He concentrations. ICRF heating at the fundamental frequency at higher helium concentrations (n_{He}/n_e = 25%) is not attractive for good single pass absorption on the helium. Second harmonic ICRF heating on the helium does give good single pass absorption, however, at these concentrations. The electron absorption is low, which is good, since it is desirable to keep the electron temperature low. Second harmonic heating on the helium would require a change in the RF generator and the antennas from those for a D-T system to accommodate the higher RF frequency.

Fuelling of a D-^{3}He plasma has been investigated for the Q $\simeq$ 1 cases. Pellet injection is difficult because of the high injection ablation rate associated with the high electron temperature. The helium content in the center of the plasma can be fuelled by neutral beam injection using a 10 MW 300 keV NBI system. Helium fuelling of the outer regions is not required since the fusion power density is strongly peaked in the center and little fusion power is produced in the outer regions. Fuelling of the deuterium in the center can also be done, but the required injection energy is also 300 keV, which requires the development of negative ion sources.

Fuelling by plasma injection, either using guns, such as the Marshall gun, or injection of compact toroid plasmas is a more speculative concept. Initial modelling of the slowing down of an injected plasma in a tokamak environment indicates that this method may be feasible. However, the experimental database for fuelling by plasma injection is almost nonexistent. Experimental investigations on the larger present tokamaks is necessary before one can have confidence in the theoretical models. Fueling by plasma injection has the advantage that it is not isotope dependent and the fuelling process appears to extrapolate to a power producing reactor.

The D-^{3}He fuel cycle produces almost all its energy in the form of charged particles; this could potentially lead to larger surface heat loads than are experienced in D-T fusion where 80% of the fusion energy is in the form of neutrons which heat the blanket and shield volumetrically. It turns out that, because of the lower fusion power density with D-^{3}He, the surface heat loads on the first wall due to bremsstrahlung and synchrotron radiation for the $Q \simeq 1$-3 cases are similar to, or less than, those encountered in the D-T version of NET. Under ignition conditions, the peak first wall heat flux will be about 100 W/cm^2, which requires a different first wall design concept. The power density on the divertor neutralizer plates due to charged particle impact is also similar to that designed for in the D-T version of NET.

From these results we see that significant energy multiplication in a mildly revised form of NET can be obtained if nature is not too perverse. Significant energy multiplication means that the fusion reactions are as important as the external heating power in determining the power balance of the plasma. Consequently, important questions regarding burn physics and the effects of a significant number of fast fusion produced ions in the plasma can be studied with such a machine. In addition, the much reduced neutron production makes the environment more hospitable to performing physics experiments on burning plasmas than is the case with DT fuel.

ACKNOWLEDGEMENTS

This research was supported by Kernforschungszentrum Karlsruhe (KfK), West Germany. The authors gratefully acknowledge helpful discussions with the NET team and valuable comments and suggestions made by W. Heeringa, K. Kleefeldt, W. Maurer, and R.A. Mueller of KfK.

REFERENCES

[1] WITTENBERG, L.J., SANTARIUS, J.F., KULCINSKI, G.L., Fusion Technology **10** (1986) 167.

[2] KULCINSKI, G.L., SANTARIUS, J.F., WITTENBERG, L.J., Clean Nuclear Power From the Moon (Proc. 1st Lunar Development Symp. Atlantic City, NJ, 1986).

[3] SANTARIUS, J.F., Nuclear Fusion **27** (1987) 167.

[4] SANTARIUS, J.F., KULCINSKI, G.L., ATTAYA, H. et al., SOAR - Space Orbiting Advanced Fusion Power Reactor, Space Nuclear Power Systems, Orbit Publishers (1987).

[5] KULCINSKI, G.L., SCHMITT, H.H., Proc. 11th Int. Scientific Forum on Fueling the 21st Century, Moscow (1987).

[6] The NET team, "NET Status Report 1985", NET Report 51, Commission of the European Communities (1985).

[7] TROYON, F., et al., Plasma Physics Cont. Fusion **5** (1980) 261.

[8] DENG, B.Q., EMMERT, G.A., Fast Ion Pressure in Fusion Plasmas, University of Wisconsin, Fusion Engineering Program, Rep. UWFDM-718 (1987).

[9] McNALLY, J. RAND, Nuclear Fusion/Technology **2** (1982) 9.

[10] TRUBNIKOV, B.A., Universal Coefficients for Synchrotron Emission from Plasma Configurations, Reviews of Plasma Physics, Plenum Press **7** (1979) 345.

[11] KAYE, S.M., GOLDSTON, R.J., Nuclear Fusion **25** (1985) 65.

[12] ATTAYA, H., SAWAN, M., NEWLIT - A General Code for Neutron Wall Loading Distribution in Toroidal Reactors, Fusion Technology **8/1** (1985) 608.

[13] TANI, K., TAKIZUKA, T., AZUMI, M., KISHIMOTO, H., Ripple Loss of Supra-thermal Alpha Particles During Slowing-Down in a Tokamak Reactor, Nucl. Fusion **23** (1983) 657.

[14] HIVELY, L.M., TF-Ripple Losses from a Non-Circular Tokamak, Nucl. Fusion **24** (1984) 779.

[15] HIVELY, L.M., Problems in Modeling TF Ripple Loss of Fast Alphas from a Tokamak Reactor, Fusion Technol. **13** (1988) 438.

[16] WITTENBERG, L.J., Helium-3 Concepts for Magnetically Confined Fusion, Proc. 12th Symp. on Fusion Energy, Monterey, CA, (1987).

[17] MILORA, S.L., FOSTER, C.A., ORNL Neutral Gas Shielding Model for Pellet-Plasma Interactions, ORNL/TM-5776 (1977).

[18] DORY, D.A., KERST, D.W., MEADE, D.M., et al., Phys. Fluids **9** (1966) 997.

[19] ADAM, J.H., Proc. 3rd I.A.E.A. Conf. on Plasma Phys. and Cont. Fusion, Novosibirsk, USSR, (1968).

[20] SCHMIDT, G., Phys. Fluids **3** (1960) 961.

[21] BAKER, D.A., HAMMEL, J., Phys. Fluids **8** (1965) 713.

[22] LEONARD, A.W., DEXTER, R.N., SPROTT, J.C., Phys. Rev. Lett. **57** (1986) 333.

[23] LEONARD, A.W., DEXTER, R.N., SPROTT, J.C., Phys. Fluids **30** (1987) 2877.

[24] HARTMAN, C.W., HAMMER, J.H., Phys. Rev. Lett. **48** (1982) 929.

[25] PERKINS, L.J., HO, S.K., HAMMER, J., Deep Penetration Fueling of Reactor-Grade Plasmas with Accelerated Compact Toroids", LLNL Rept. UCRL-96894 (1987).

[26] TIBER II/ETR Final Design Report, ed. by J.D. Lee, LLNL Rept. UCID-21150 Vol. 1, (1987).

[27] SCHARER, J., JACQUINOT, J., LALLIA, P., SAND, F., Fokker-Planck Calculations for JET ICRF Heating Scenarios," Nuclear Fusion **25** (1985) 435.

[28] HARVEY, KERBEL, McCOY, ChIU, ICRF Fusion Reactivity Enhancement in Tokamaks, Nuclear Fusion **26** (1986) 43.

[29] JET Team, RF Heating on JET," Int. Conf. on Plasma Physics and Controlled Fusion Research, Kyoto, Japan, IAEA-CN-47/F-I-1 (1986).

[30] HOSEA, J., et al., 12th European Conf. on Controlled Fusion and Plasma Physics, Budapest, Hungary, 9F Part II (1985) 120.

[31] SADLER, G., JARVIS, O., BELLE, P., HAWKES, N., SYRNE, B., Observation of Fusion Reaction γ-Rays in JET, Proc. of European Conf. on Plasma Physics and Controlled Fusion, Madrid (1987) 1232.

[32] McVEY, B., SUND, R., SCHARER, J., Local Power Conservation for Linear Wave Propagation in an Inhomogeneous Plasma, Phys. Review Letters (1985) 507.

TABLE I. MAIN CONFIGURATIONAL AND PLASMA PARAMETERS OF THE NET REFERENCE OPTIONS NET-DT AND NET-EP

		NET-DT	NET-EP
Plasma major radius	R (m)	5.18	5.41
Plasma minor radius	a (m)	1.35	1.68
Plasma elongation	b/a	2.18	2.17
Aspect ratio	A=R/a	3.8	3.2
Magnetic field on axis	B (T)	5.0	4.8
maximum on coils	B_m (T)	10.4	(10.4)
Plasma current	I_p (MA)	10.8	14.8
Fusion power	P_{fus} (MW)	600	1000

TABLE II. SUMMARY OF D-^{3}He NET OPTIMUM OPERATING PARAMETERS USING ASDEX H-MODE SCALING

	Case							
	A-1	A-2	A-3	B-1	B-2	C-1	D-1	D-2
Major Plasma Radius, m	5.18	5.41	5.14	4.61	4.61	5.41	4.61	4.61
B at Magnet, T	10.4	10.4	10.4	10.4	10.4	13	10.5	13
B at Plasma, T	4.96	4.75	5.0	5.57	5.57	5.93	5.63	6.97
Q	.96	1.4	1.15	3.06	.95	2.8	∞	∞
P_{inj}, MW	35	37	53	32	84	38	0	0
Plasma Current, MA	10.8	14.8	16.2	20.2	20.2	18.3	29.6	29.5
Elongation	2.17	2.17	2.17	2.17	2.17	2.17	2.7	2.38
Deuterium Fraction	.65	.65	.65	.65	.34	.65	.65	.65
$\langle n_i \rangle$, 10^{13} cm^{-3}	3.6	3.5	4.6	4.7	6.0	4.6	8.8	10.7
$\langle T_i \rangle$, keV	45	45	37	51	37	51	37	37
$\langle T_e \rangle$, keV	28	31	28	37	30	37	34	34
$\langle \beta \rangle$	.056	.064	.067	.075	.075	.064	.11	.088
Energy Confinement Time, s	5.6	7.9	8.3	9.3	9.3	9.9	13.6	13.6
Inboard Shield, cm	116	100	70	29	29	100	29	29
<Neutron Wall Load>, MW/m^2	.004	.006	.016	.016	.002	.016	.055	.08
Photon Heat Flux to Wall, W/cm^2	4.5	5.9	9.9	14.5	20.9	15	31	50
Fusion Power, MW	34	53	61	98	79	108	240	286
Neutron Power, MW	0.9	1.9	7.8	4.9	0.67	5.7	21.9	28.6
Power to Divertor, MW	53	62	69	71	79	76	94	103
τ_p/τ_E	1	1	4	1	1	1	1	1
Oxygen Impurity Concent. (%)	0	0	1	0	0	0	0	0

TABLE III. COMPARISON BETWEEN THE RADIATION EFFECTS AT THE TF COILS

$\Gamma_{i/b}$ (MW/m^2)	0.0193
Total Nuclear Heating in 16 TF Coils (kW)	13.3
Peak Dose in GFF epoxy (rad @ 2.32 FPD)	0.1×10^8
Peak Nuclear Heating in Winding Pack (mW/cm^3)	1.2
Peak dpa in Cu Stabilizer (dpa @ 2.32 FPD)	1.1×10^{-5}
End-of-Life Radiation Induced Resistivity (nΩm)	7.9×10^{-3}
Peak Fast Neutron Fluence (n/cm^2 @ 2.32 FPD)	1.7×10^{16}

TABLE IV. RADIATION EFFECTS IN THE INNER AND OUTER LEGS OF THE TF MAGNETS

	Inboard	Outboard
$\hat{r}_n$ (MW/m^2)	0.0155	0.0145
Shield Thickness (cm)	70	59
Coil Case Thickness (cm)	--	9.4
Nuclear Heating in		
Winding Pack (kW)	0.12	0.45
Coil Case (kW)	--	0.78
Peak Nuclear Heating in Winding Pack (mW/cm^3)	1.3×10^{-2}	1.25×10^{-2}
Peak Dose to GFF Epoxy (rad @ 2.32 FPD)	7.8×10^{4}	9.2×10^{4}
Peak Fast n Fluence (n/cm^2 @ 2.32 FPD)	5.3×10^{13}	1.2×10^{14}
Peak dpa in Cu Stabilizer (dpa @ 2.32 FPD)	4.0×10^{-8}	7.1×10^{-8}

TABLE V. FIRST WALL HEAT FLUX

	CASE							
	A-1	A-2	A-3	B-1	B-2	C-1	D-1	D-2
Major Radius, m	5.18	5.41	5.14	4.61	4.61	5.41	4.61	4.61
Minor Radius, m	1.35	1.69	1.69	1.69	1.69	1.69	1.69	1.69
Plasma Area, m^2	362	475	450	405	405	475	472	431
Synchrotron Power, MW	9.1	16	17	37	29	47	54	90
Bremsstrahlung, MW	7.3	12	29	22	56	24	92	124
Neutron Wall Load Peaking								
Inboard	1.1	1.1	1.5	1.7	1.7	1.7	1.7	1.7
Outboard	1.5	1.5	1.4	1.3	1.3	1.3	1.3	1.3
Heat Flux								
Average, W/cm^2	4.5	5.9	10	15	21	15	31	50
Peak Inboard, W/cm^2	7.6	11	20	38	46	34	69	114
Peak Outboard, W/cm^2	4.4	5.5	11	11	21	12	31	47

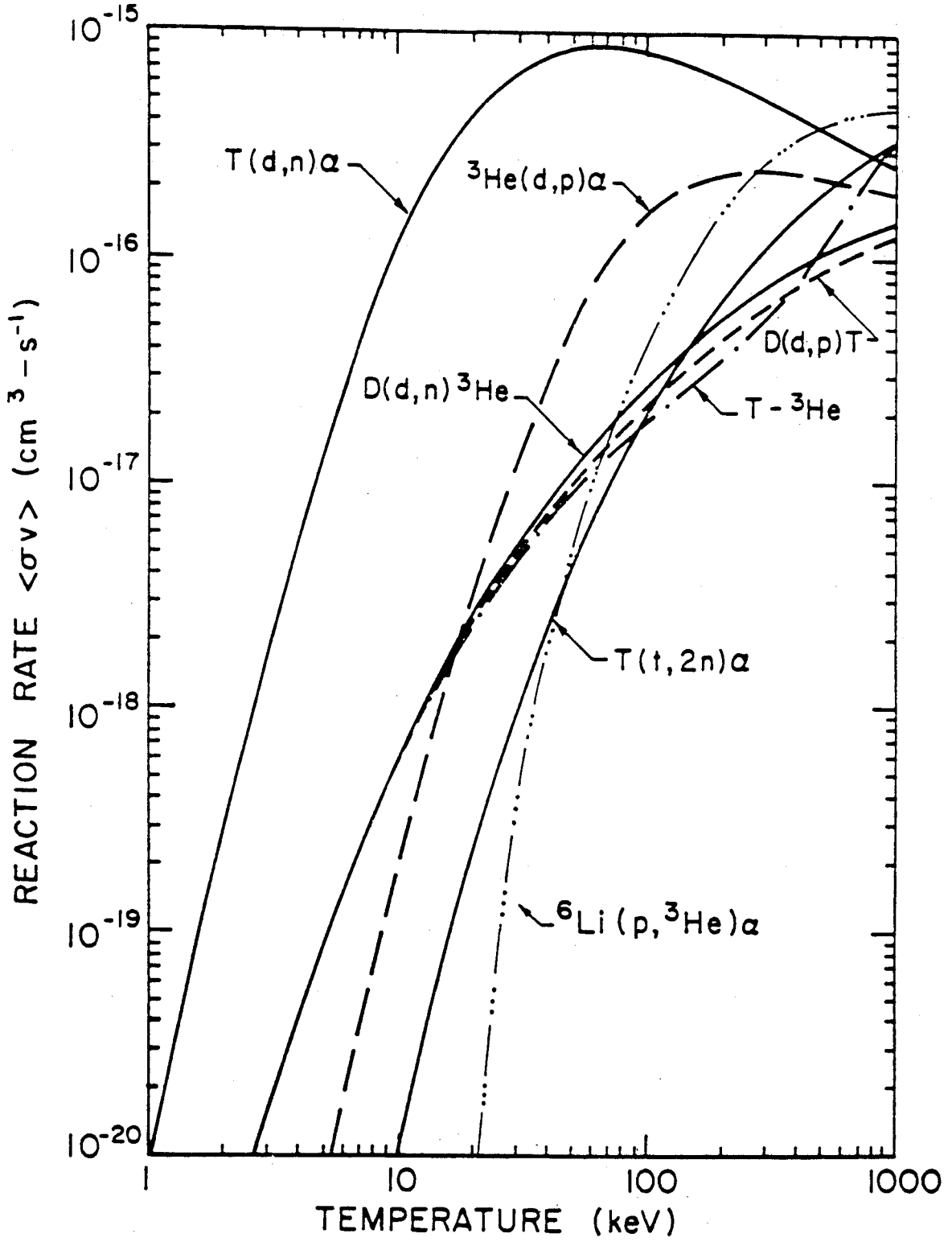

Fig. 1. The Maxwellian averaged reaction rate, $\langle\sigma v\rangle_f$, as a function of ion temperature for various fusion reactions.

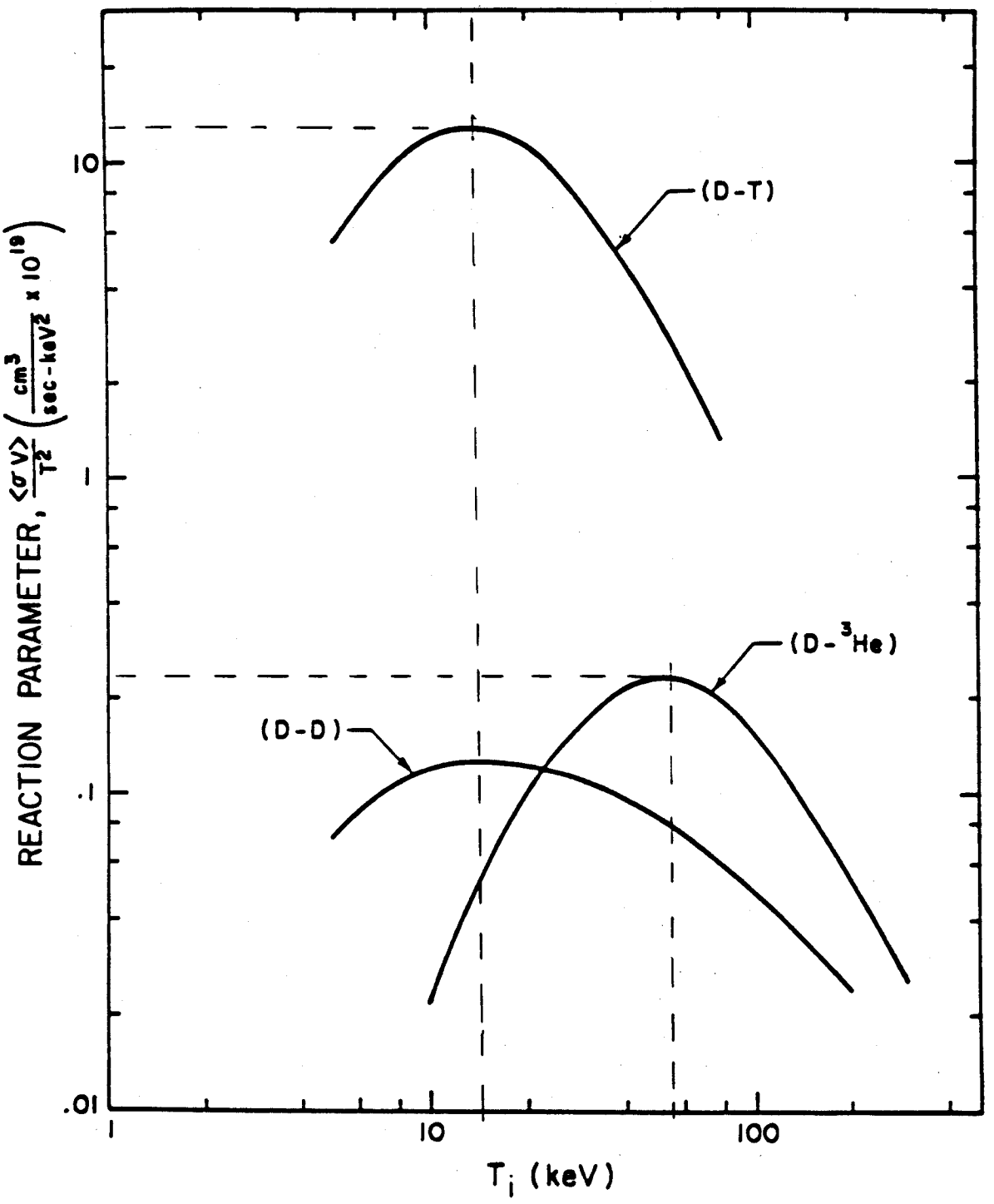

Fig. 2. The Maxwellian averaged reaction rate parameter, $\langle\sigma v\rangle/T^2$, as a function of ion temperature for several fusion fuel cycles.

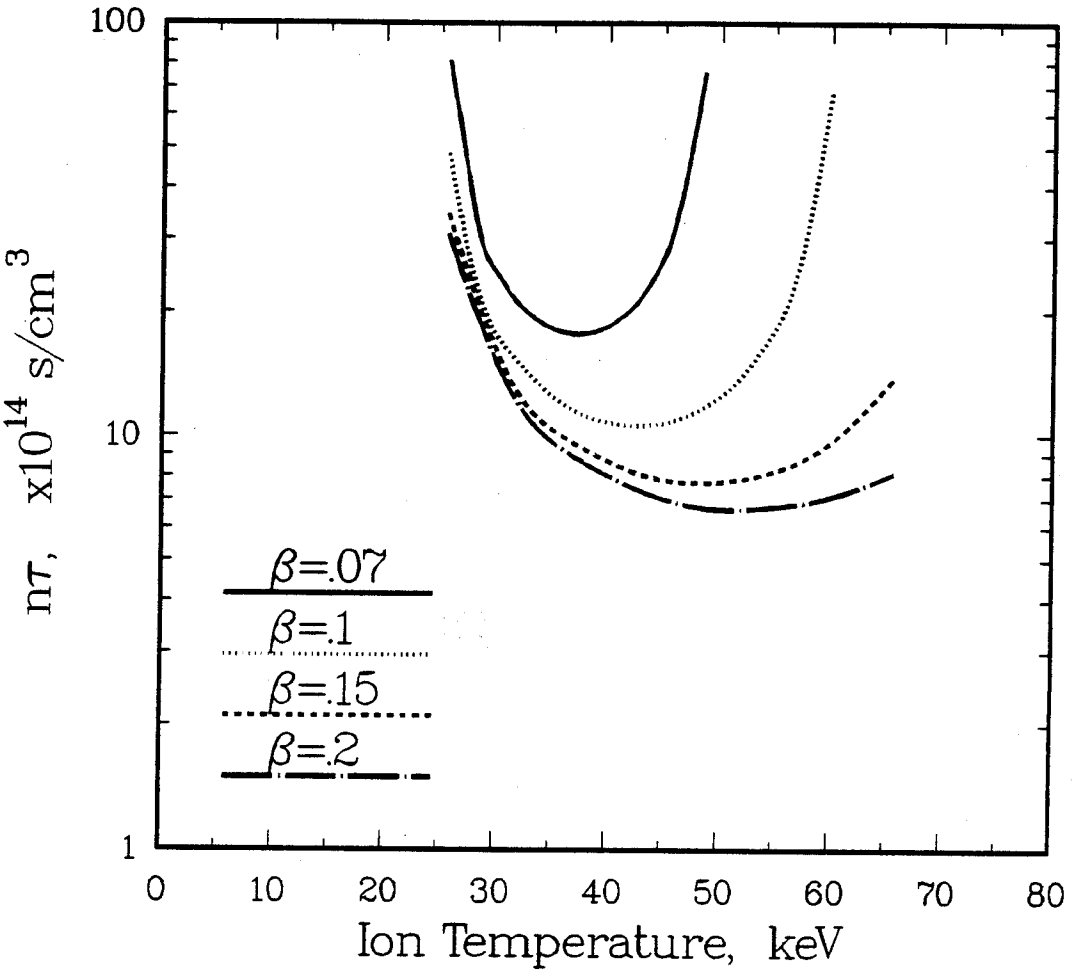

Fig. 3. Lawson parameter for D-^{3}He versus volume-averaged ion temperature.

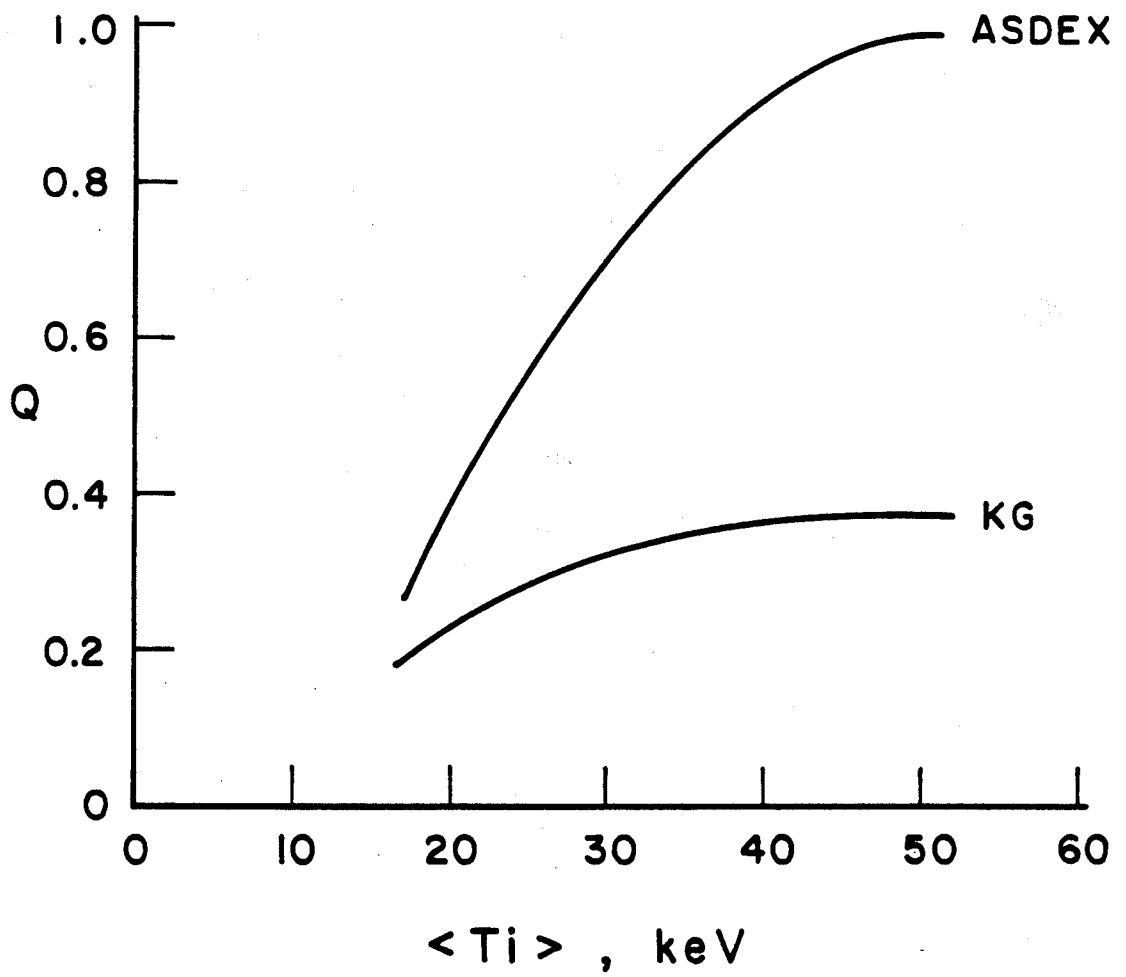

Fig. 4. Energy multiplication, Q, versus average ion temperature for D-^{3}He operation in NET-DT for both ASDEX H-mode and Kaye-Goldston energy confinement scaling.

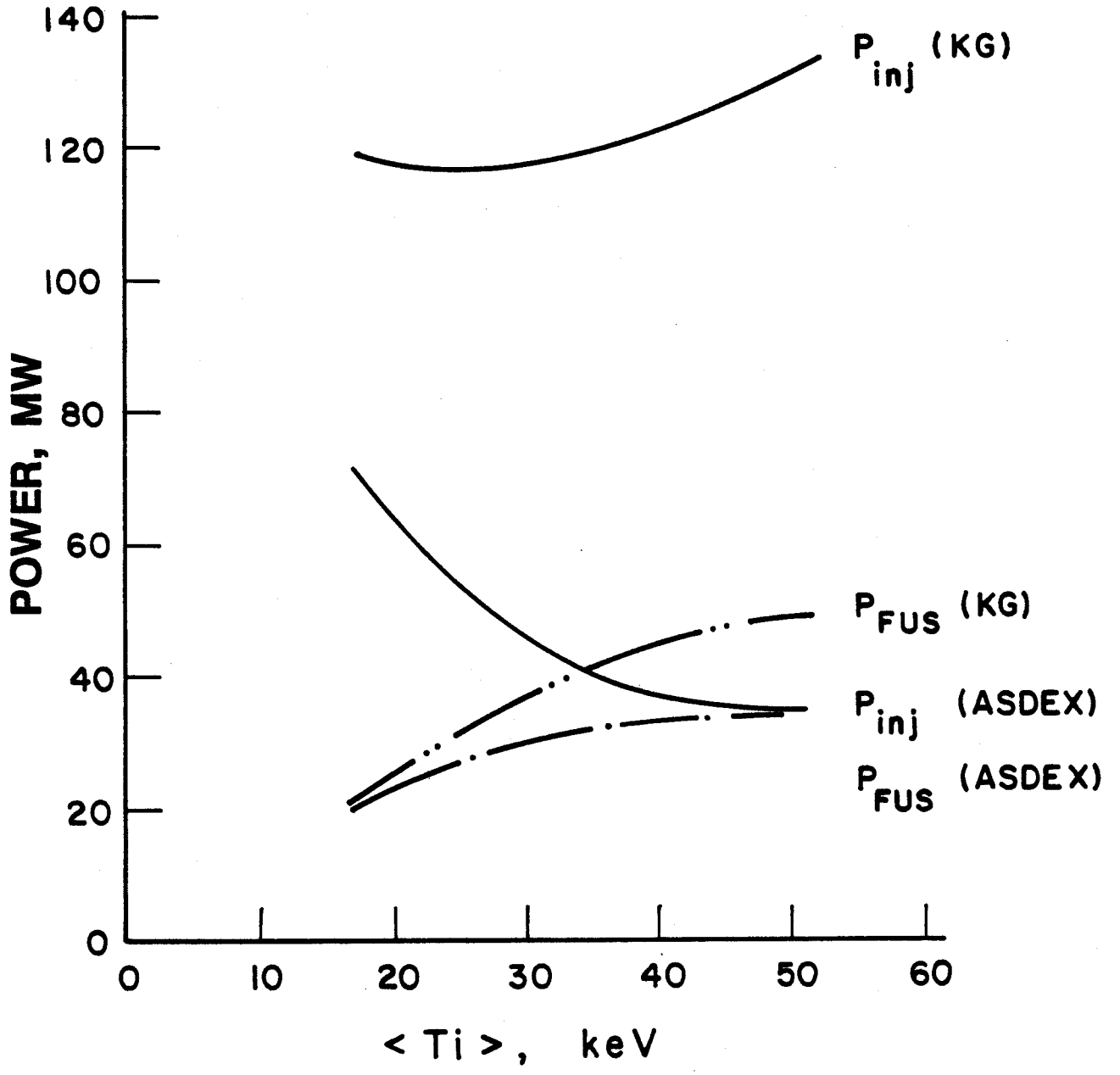

Fig. 5. Injection power and fusion power versus average ion temperature for NET-DT for both ASDEX H-mode and Kaye-Goldston energy confinement scaling.

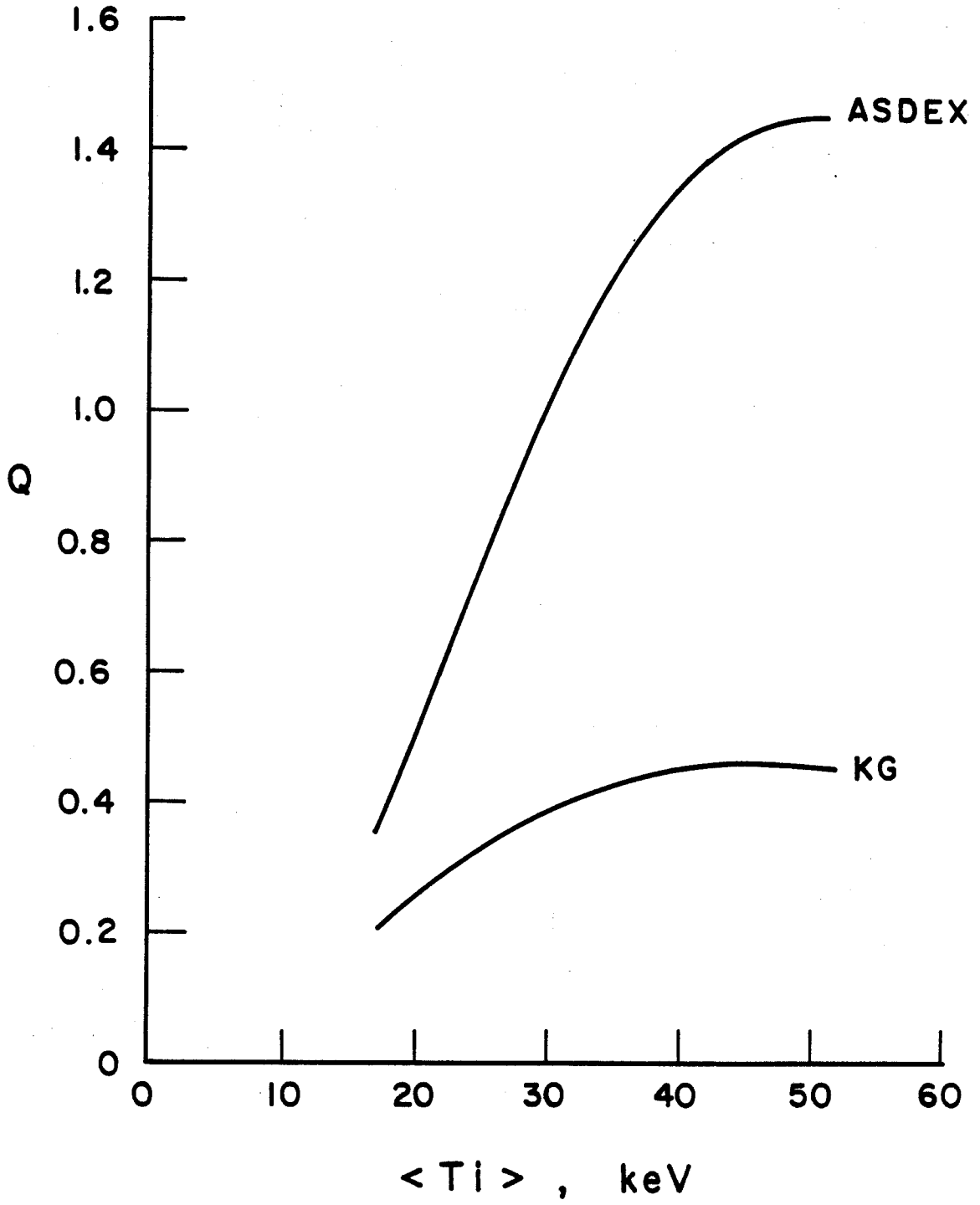

Fig. 6. Energy multiplication, Q, versus average ion temperature for NET-EP for both ASDEX H-mode and Kaye-Goldston energy confinement scaling.

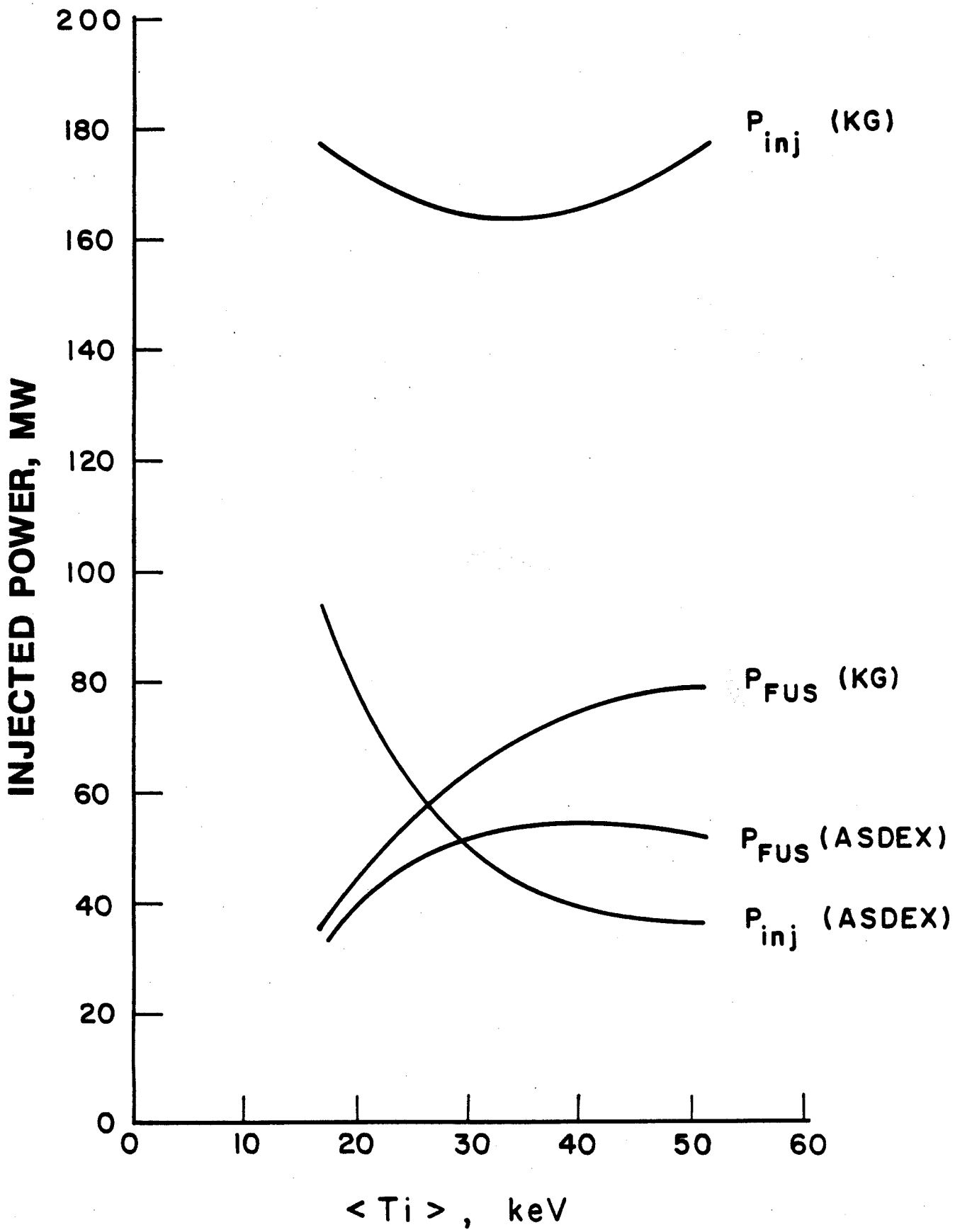

Fig. 7. Injection power and fusion power versus average ion temperature for NET-EP for both ASDEX H-mode and Kaye-Goldston energy confinement scaling.

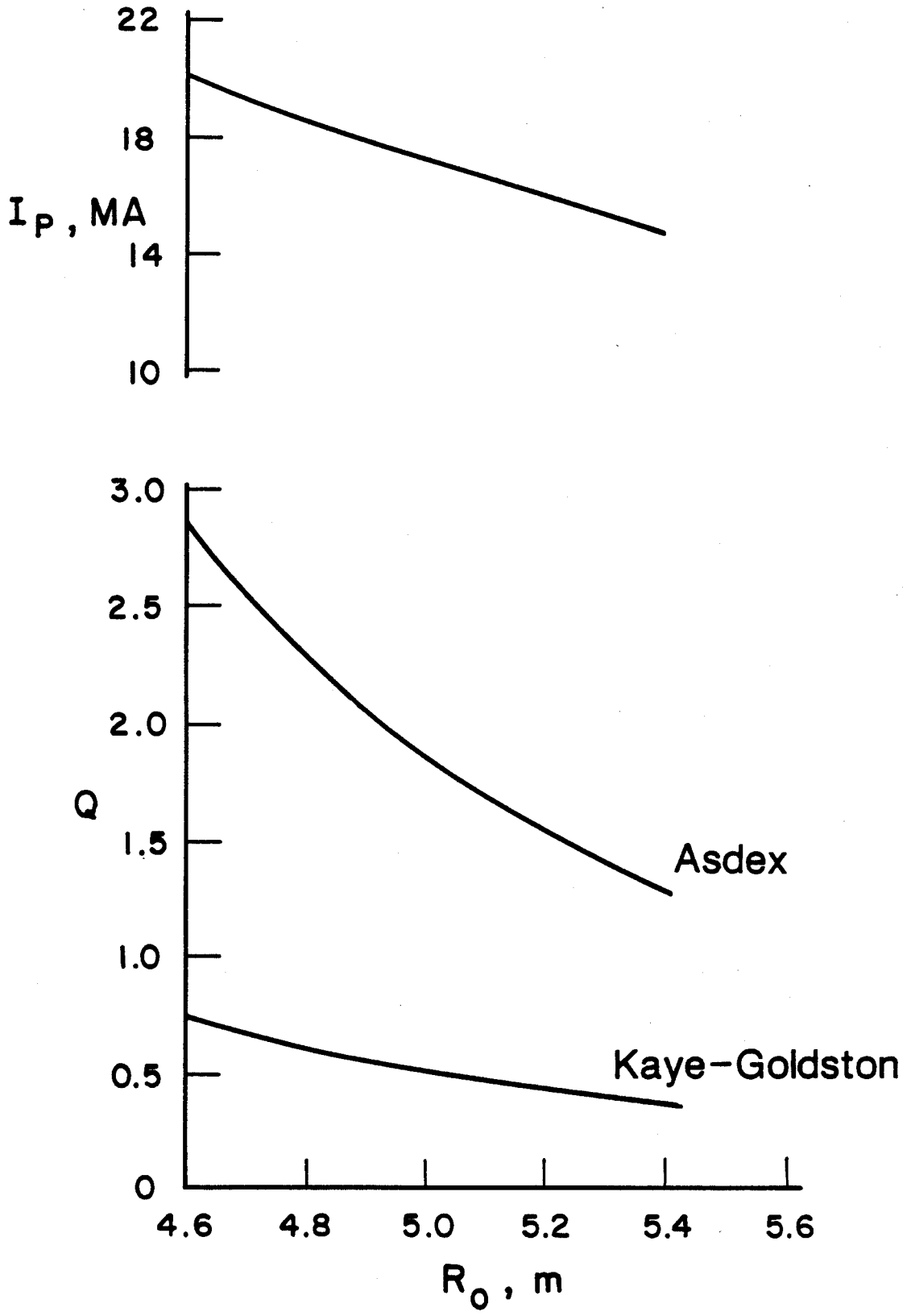

Fig. 8. Q and plasma current versus major radius; a = 1.69 m, B_c = 10.4 T, K = 2.17, $\langle T_i \rangle$ = 37 keV.

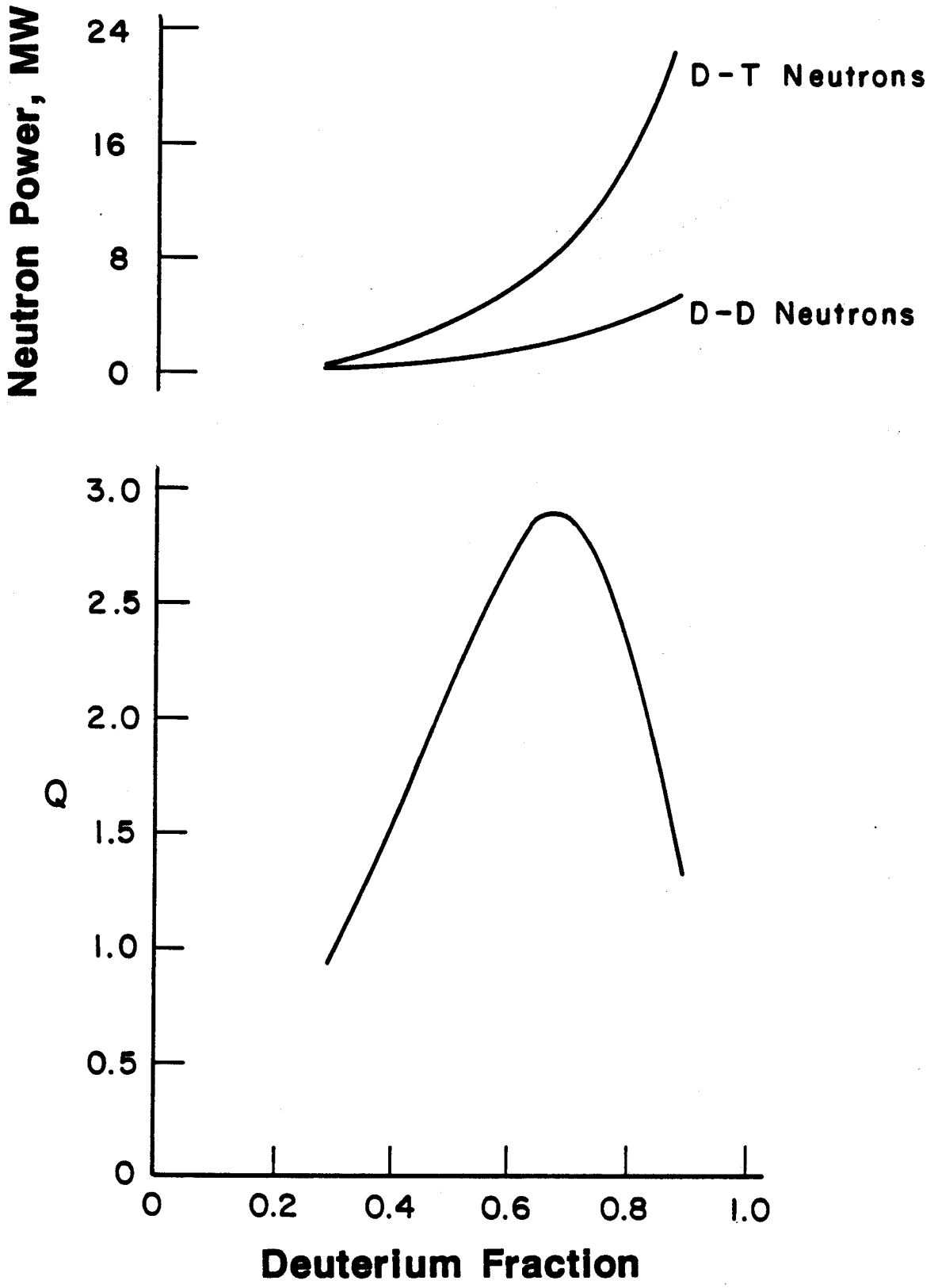

Fig. 9. Effect of changing fuel mixture on the energy multiplication, Q, and neutron power. R = 4.61 m, B_c = 10.4 T, $\langle T_i \rangle$ = 37 keV, ASDEX H-mode scaling.

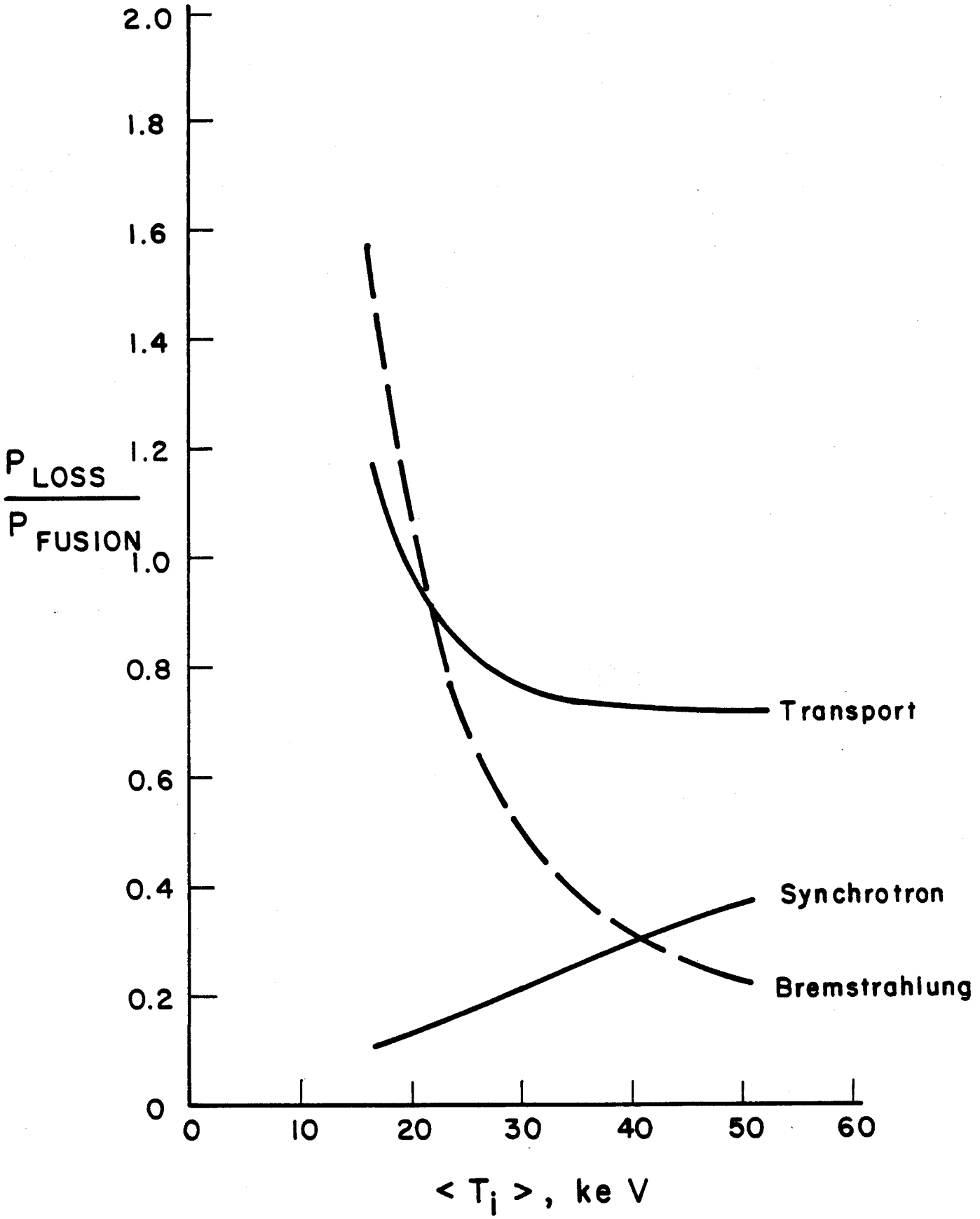

Fig. 10. Distribution of power loss versus average ion temperature. R = 4.61 m, B_c = 10.4 T, f_d = .65, ASDEX H-mode scaling.

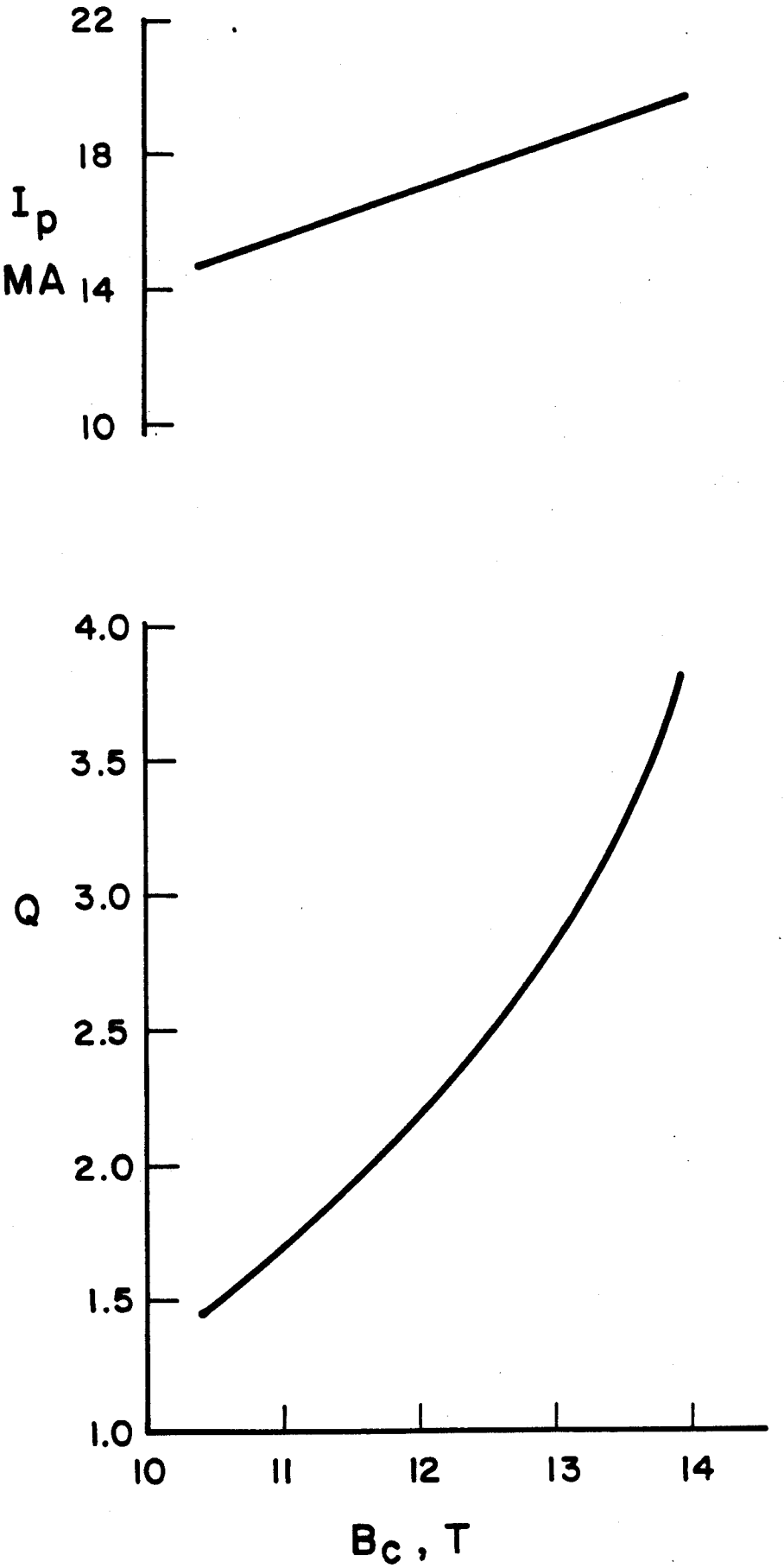

Fig. 11. The effect of raising the toroidal field at the magnet on the energy multiplication, Q, and the plasma current, I_p. R = 5.41 m, f_d = .65, $\langle T_i \rangle$ = 50 keV.

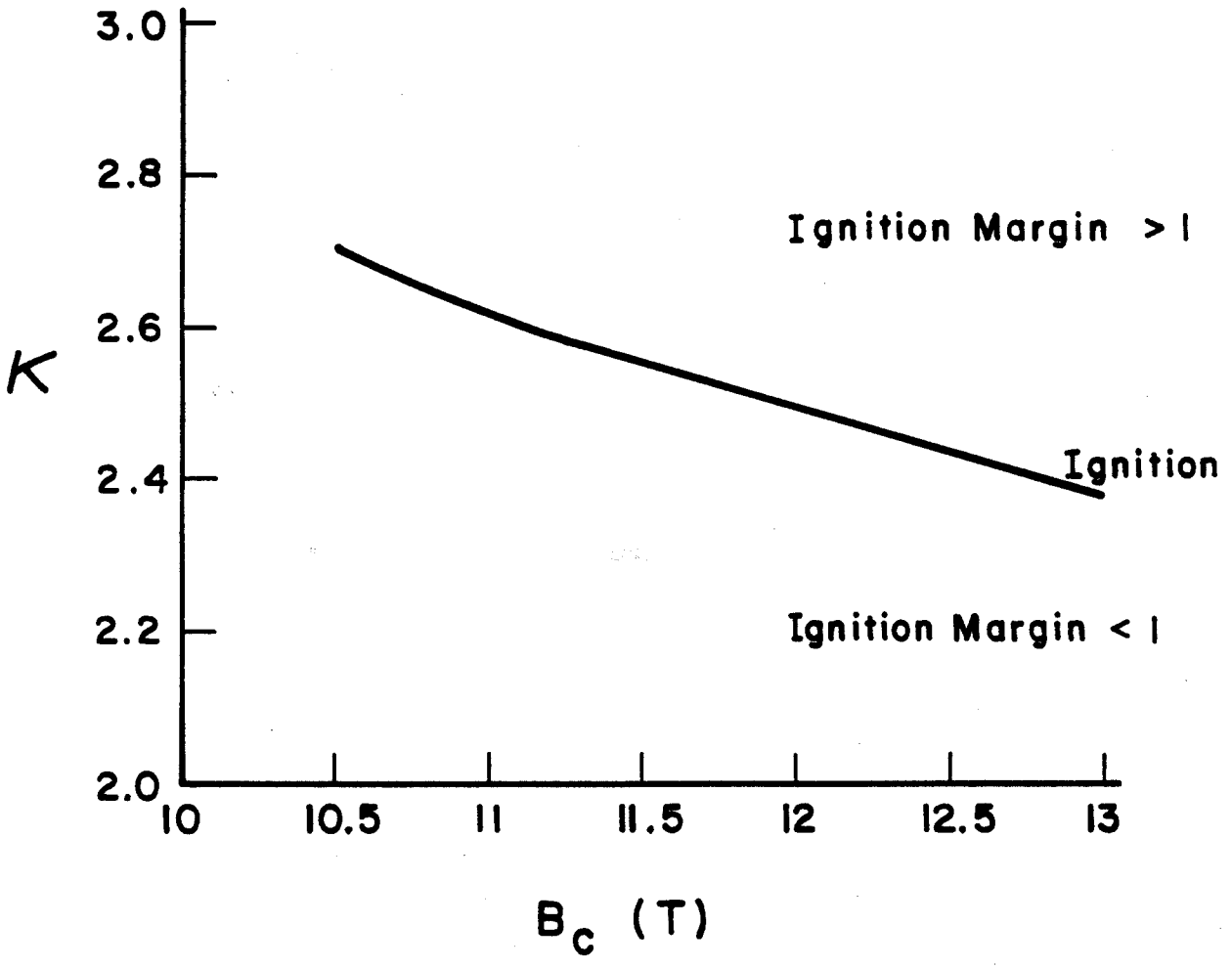

Fig. 12. The elongation required to achieve ignition versus toroidal magnetic field at the magnet. Points above the curve have ignition margin above 1; points below are subignited. R = 4.61m, a = 1.69 m, $\langle T_i \rangle$ = 37 keV, ASDEX H-mode scaling.

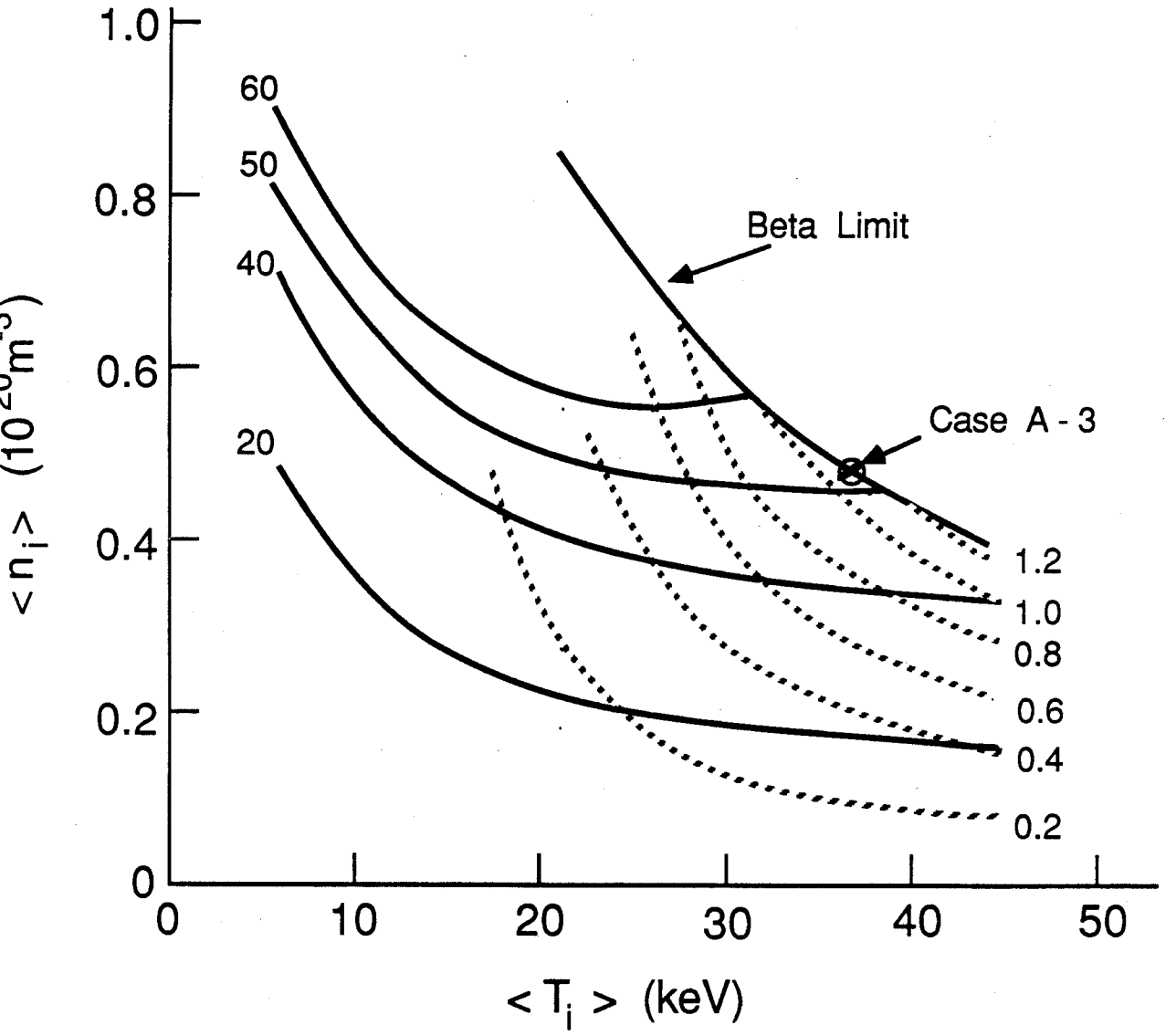

Fig. 13. Density-temperature operating space for case A-3 using ASDEX H-mode scaling. The solid lines are constant injected power (MW) and the dotted lines are constant Q.

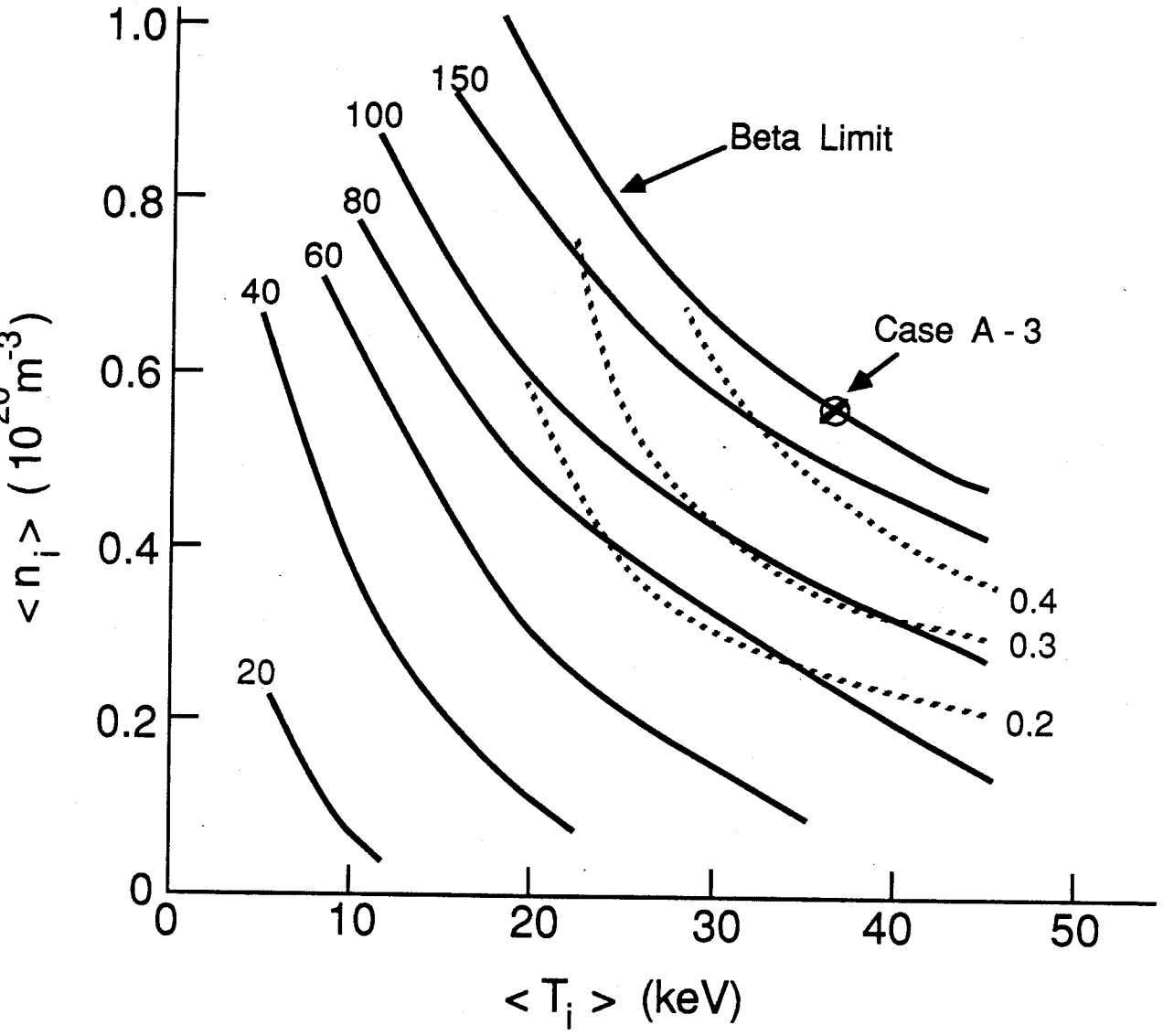

Fig. 14. Density-temperature operating space for case A-3 using Kaye-Goldston scaling with an H-mode factor of 2. The solid lines are constant injected power (MW) and the dotted lines are constant Q.

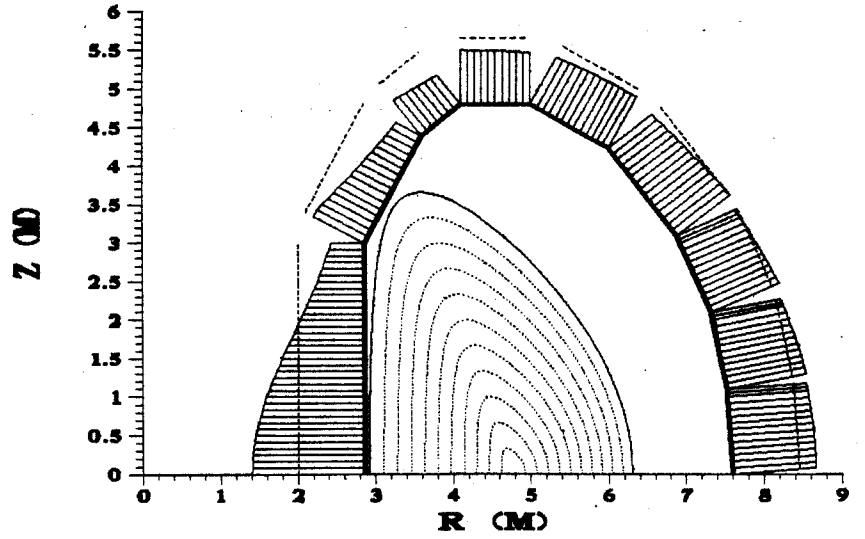

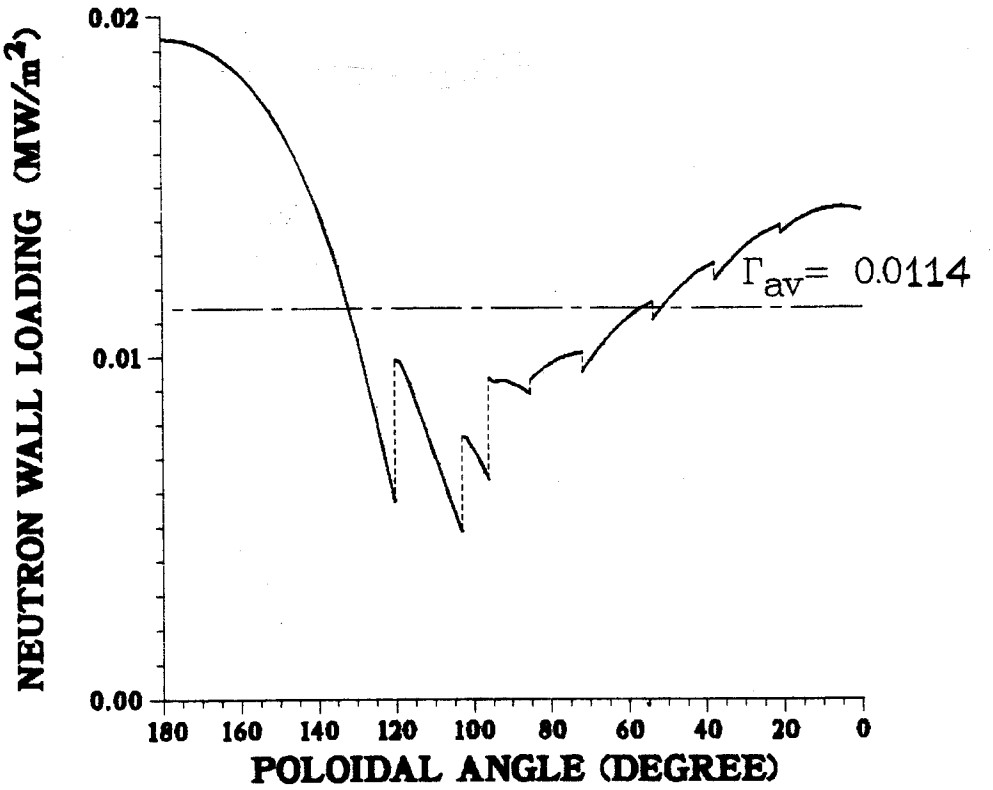

Fig. 15. Poloidal variation of the neutron wall loading in NET-D^{3}He reactor (case B-1 with lower ion temperature).

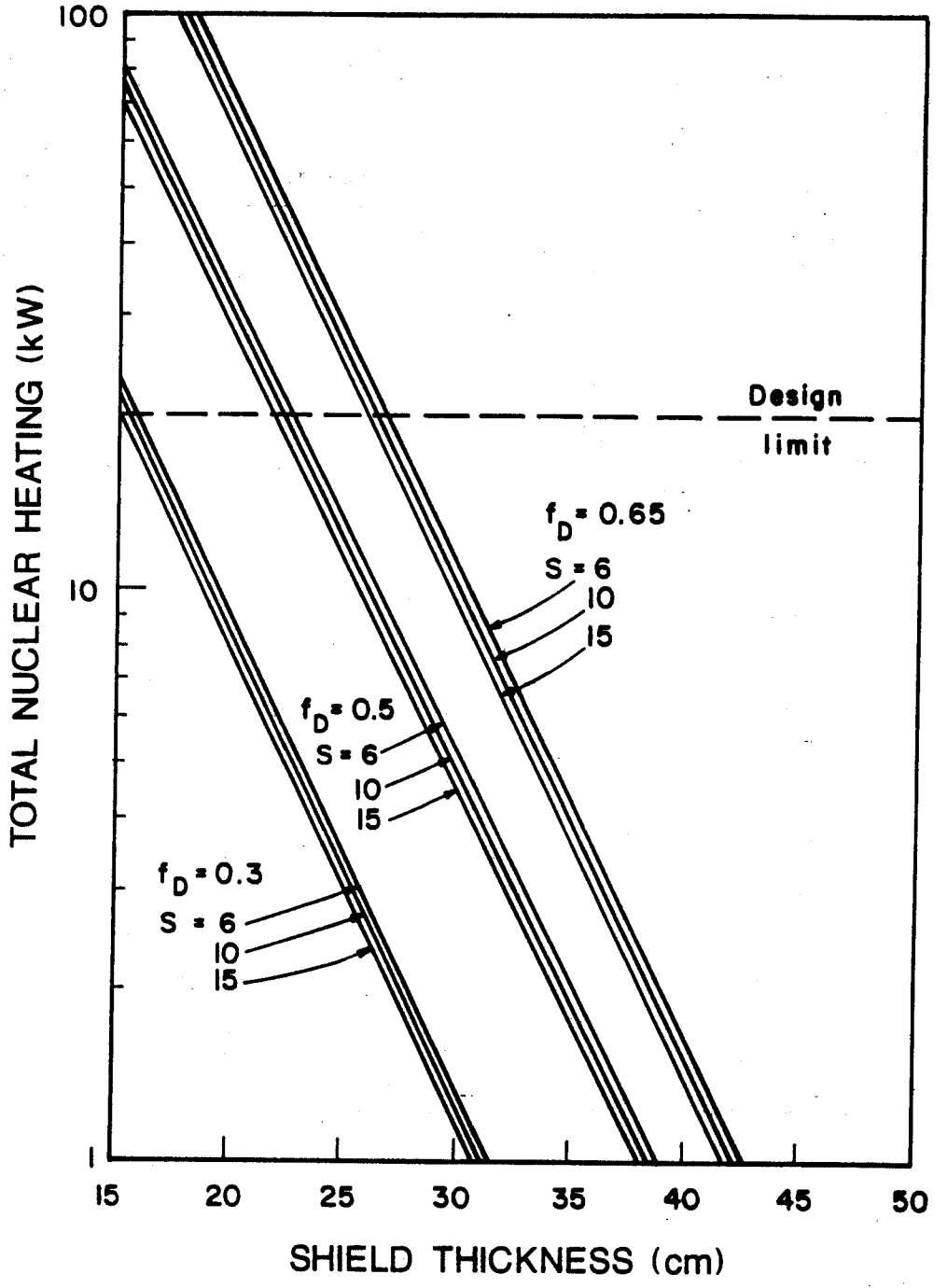

Fig. 16. Variation of the total nuclear heating in the 16 TF coils with the i/b shield thickness.

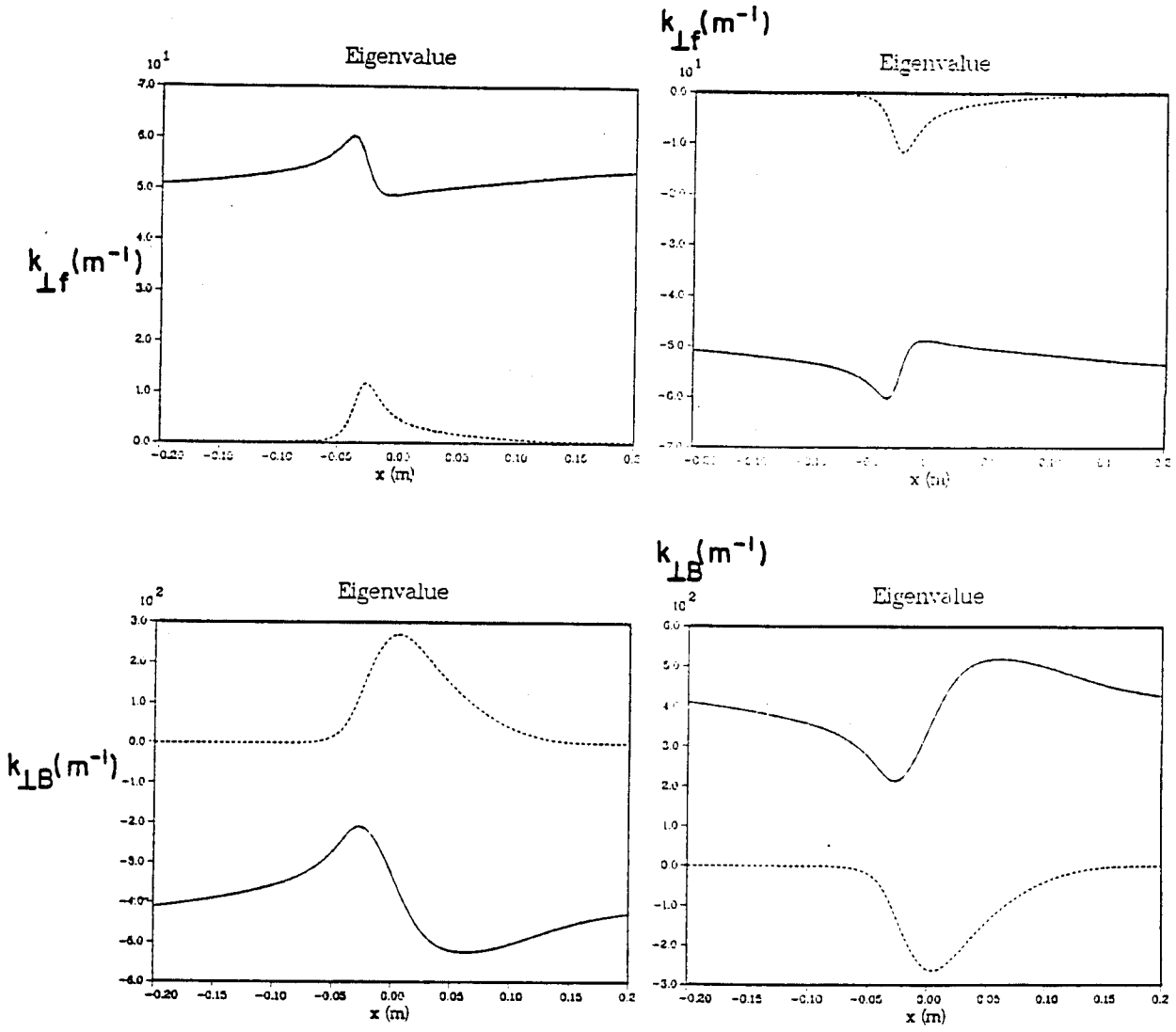

Fig. 17. Fast (F) and ion Bernstein wave (P) dispersion for fundamental ^3He heating in NET-EP.

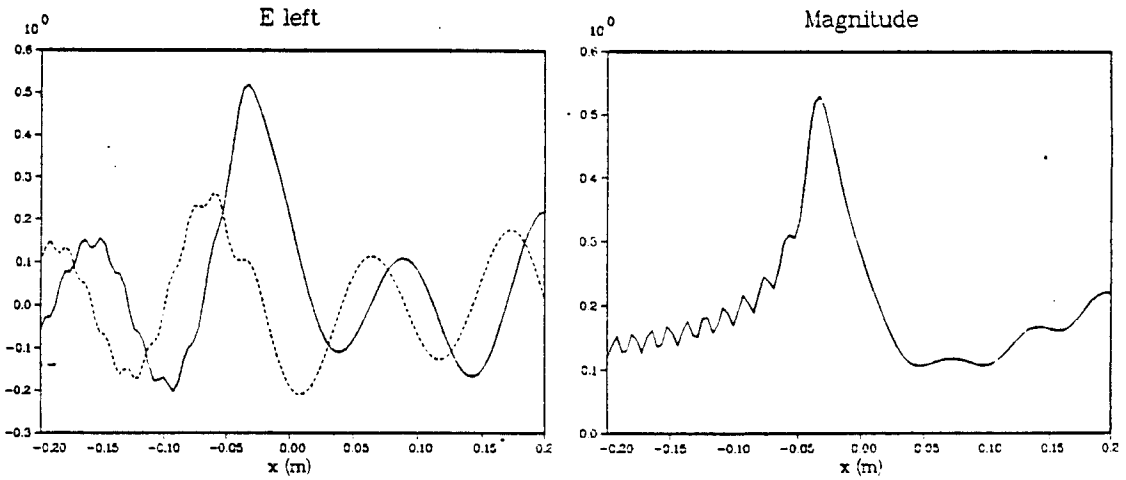

Fig. 18 Left hand wave polarization for NET-EP parameters.

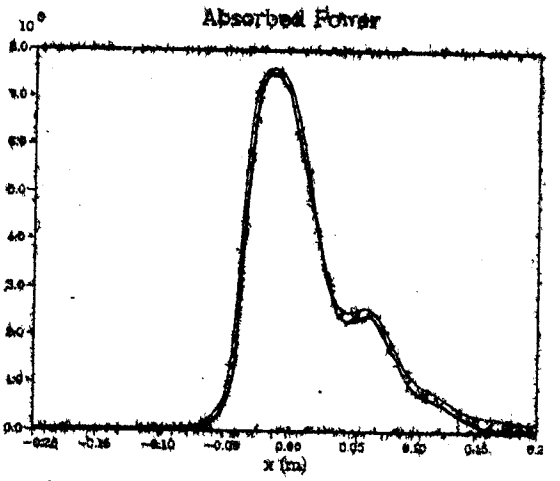

(a)

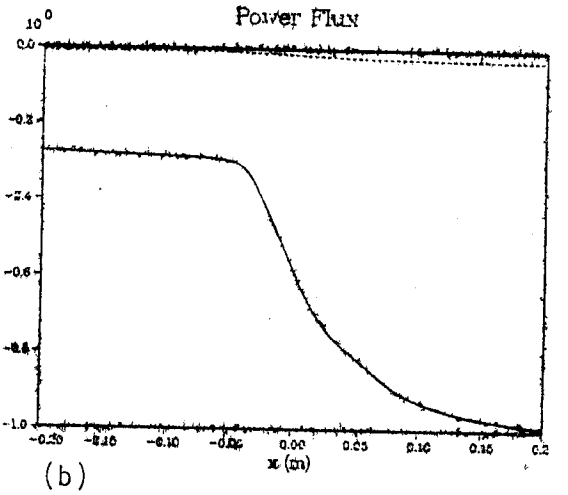

(b)

Fig. 19. (a) Helium and electron (hatched) fast wave absorption for NET-EP parameters.
(b) Poynting (solid) and kinetic flux for a fast wave incident from the right for NET-EP parameters.